Journal of Nuclear Medicine, published on November 18, 2021 as doi:10.2967/jnumed.121.262992

Combination of carriers, with complementary intratumoral microdistributions of delivered α-particles, may realize the promise for Actinium-225 in large solid tumors

Alaina Howe[1,‡], Omkar Bhatavdekar[1,†], Dominick Salerno[1,†], Anders Josefsson[2], Jesus Pacheco-Torres[2], Zaver M. Bhujwalla[2], Kathleen L. Gabrielson[3], George Sgouros[2], Stavroula Sofou[1,4*]

[1]Chemical and Biomolecular Engineering (ChemBE), Institute for NanoBioTechnology (INBT)

[2] Russell H. Morgan Department of Radiology and Radiological Science

[3]Molecular and Comparative Pathobiology

[4]Sidney Kimmel Comprehensive Cancer Center, Cancer Invasion & Metastasis Program, Department of Oncology,

Johns Hopkins University, Baltimore, MD

[†]equally contributing authors

[*]corresponding author

ChemBE, Johns Hopkins University

3400 North Charles Street

Maryland Hall 221

Baltimore, MD 21218

phone: 410-516-0274

fax: 410-516-5510

email: ssofou1@jhu.edu

‡graduate student in training

ChemBE, Johns Hopkins University

3400 North Charles Street

Croft Hall B20

Baltimore, MD 21218

phone: 410-516-7143

fax: 410-516-5510

email: ahowe5@jhu.edu

Word Count: 5115

Running Title: α-particle radiotherapy for solid tumors

ABSTRACT

Alpha-particle radiotherapy has already been shown to be impervious to most resistance mechanisms. However, in established (i.e. large, vascularized) soft-tissue lesions, the diffusion-limited penetration depths of radiolabeled antibodies and/or nanocarriers (up to 50-80μm) combined with the short range of α-particles (4-5 cell diameters) may result in only partial tumor irradiation potentially limiting treatment efficacy. To address this challenge, we combined carriers with complementary intratumoral microdistributions of the delivered α-particles. We use the α-particle generator Actinium-225 (^{225}Ac), and we combine (1) a tumor-responsive liposome that upon tumor uptake releases in the interstitium a highly-diffusing form of its radioactive payload (^{225}Ac-DOTA), which may penetrate the deeper parts of tumors where antibodies do not reach, with (2) a separately administered, less-penetrating radiolabeled-antibody irradiating the tumor perivascular regions from where liposome contents clear too fast. **Methods:** On a murine model with orthotopic HER2-positive BT474 breast cancer xenografts, the biodistributions of each carrier were evaluated, and the control of tumor growth was monitored after administration of the same total radioactivity of ^{225}Ac delivered (1) by the ^{225}Ac-DOTA-encapsulating liposomes, (2) by the ^{225}Ac-DOTA-SCN-labeled-trastuzumab, and (3) by both carriers at equally split radioactivities. **Results:** Tumor growth inhibition was significantly more pronounced when the same total injected radioactivity was divided between the two separate carriers, as compared to the growth delay by the same total injected radioactivity when delivered by either of the carriers alone. The combined carriers enabled more uniform intratumoral microdistributions of α-particles, at a tumor delivered dose that was lower than the dose delivered by the antibody alone. **Significance:** This strategy demonstrates that more uniform microdistributions of the delivered α-particles within established solid tumors improve efficacy even at lower tumor delivered doses. Augmentation of antibody-targeted α-particle therapies with tumor-responsive liposomes may address partial tumor irradiation improving therapeutic effects.

Key words: Actinium-225, liposomes, antibodies, tumor microdistributions

INTRODUCTION

Metastatic and/or recurrent solid cancers present an all too common clinical challenge partly due to development of resistance (*1*). Clinical studies with α-particle emitters have sometimes had exceptional outcomes on patients with metastatic prostate cancer resistant to approved options (*2,3*). The promise of α-particles targeted via antibodies against advanced cancers (not limited to prostate cancer) is currently under investigation in clinical studies. An effective and tolerable α-particle based treatment against established (i.e. large, vascularized) lesions is critical to successfully handling solid tumor patients with advanced disease that is resistant to established approaches.

Alpha-particle radiotherapy has already been shown, across a diverse panel of tumor cells, to be impervious to most resistance mechanisms, in the absence of transport barriers; cells most resistant to γ radiation have been reported to be sensitive to α-particles (*4*). The complexity and level of double-strand DNA damage caused by only a few tracks of α-particles across the cell nucleus overwhelms cellular repair mechanisms mostly independently of the cell-oxygenation state and cell-cycle (*5*); this inability to repair lethal damage is the reason that α-particle therapy, if optimally delivered, is impervious to resistance. However, the short range of α-particles (40-100 μm), which is ideal for localized irradiation and minimal irradiation of surrounding healthy tissues, also limits penetration within large tumors; the diffusion-limited penetration depths (up to 50–80μm) of established and alternative vectors, such as radiolabeled antibodies and/or nanocarriers, respectively, combined with the short range of α-particles may result in only partial tumor irradiation (*6*). Importantly, partial tumor irradiation may limit the treatment efficacy of α-particle therapies irrespective of any augmenting by-stander effects (*7*).

Tumor-selective delivery strategies for α-particle therapies that aim to spread the intratumoral α-particle distributions over larger regions within solid tumors, and to prolong exposure of cancer cells to delivered radiotherapeutics, may improve efficacy against established tumors**.** Toward this goal, we

evaluated a strategy to deliver the α-particle generator Actinium-225 (^{225}Ac) as uniformly as possible throughout established tumors using a human epidermal growth factor receptor 2 (HER2)-positive human breast cancer, chosen as a model tumor for proof-of-concept. We combined two different delivery carriers of ^{225}Ac, tumor-responsive liposomes and HER2-targeting antibodies, each administered separately. The liposomes were engineered to have two key properties for the implementation of our strategy: (1) to clear slowly from tumors and, (2) only in the tumor interstitium, to release highly diffusing forms (due to their small size) of the α-particle emitters (^{225}Ac-DOTA) which then may penetrate in the deep parts of tumors, where antibodies do not reach (*6*). The antibodies were also labeled with ^{225}Ac, which they deliver mostly closer to the tumor periphery (the perivascular regions), where the liposome-based modality suffers due to fast clearance of released therapeutic agents (*8*).

The tumor-responsive liposomes were designed to exhibit the following properties, all of which were triggered by the slightly acidic pH in the tumor interstitium (pH_e~6.7-6.5)(*9*): (1) adherence to the tumors' extracellular matrix (resulting in slower liposome clearance from the tumor (*8*)), (2) low uptake and/or internalization by cancer cells (*8*), and, (3) release of contents directly in the interstitium triggered by the tumor acidity (*6*). The HER2-targeting antibody, trastuzumab, that was administered separately from liposomes, was chosen because of its high affinity for the HER2 receptor, reasonable radiolabeling and well-characterized *in vivo* behavior.

Herein, we evaluate our hypothesis that combination of different carriers that deliver α-particle radiotherapies to complementary regions of the same solid tumor result in more uniform irradiation over a larger fraction of the solid tumor’s volume and, therefore, in greater tumor growth inhibition compared to the same administered radioactivity delivered by each carrier alone.

MATERIALS AND METHODS

Materials

All materials are described in Supplemental Information. Actinium-225 (^{225}Ac, actinium chloride) was supplied by the U.S. Department of Energy Isotope Program, managed by the Office of Isotope R&D and Production.

Liposome Formation and Characterization

Tumor-responsive liposomes, composed of 20PC:DPPS:cholesterol:DSPE-PEG-DAP:DPPE-Rhodamine at 0.61:0.26:0.04:0.09:0.001 mole ratio, were formed using the thin-film hydration method as described in detail in the Supplemental Information (*6*). Liposomes were characterized for size and zeta potential using a Zetasizer NanoZS90 (Malvern, United Kingdom).

Radiolabeling of Carriers with ^{225}Ac/^{111}In

DOTA-SCN-trastuzumab (and/or DTPA-SCN-trastuzumab) was radiolabeled and characterized as described in Supplemental Information (*6*). Liposomes encapsulating DOTA (or DTPA) were loaded with ^{225}Ac (or ^{111}In) using the ionophore A23187 (*6*).

Cell Culture

BT474 and the trastuzumab-resistant BT474 (BT474-R) were obtained from American Type Culture Collection and were grown in cell culture treated flasks at 37°C and 5% CO_2 in Hybricare media buffered with sodium bicarbonate supplemented with 10% fetal bovine serum, 100U/mL penicillin and 100mg/mL streptomycin.

Clonogenic Survival

After incubation for 6 hours of cell monolayers with varying concentrations of radioactivity, the cells were washed and were plated in dishes to grow until formation of colonies, as described in detail in the Supplemental Information.

Spheroid Formation and Spatiotemporal Profiles

BT474 cells were seeded on polyHEMA-coated, 96-well round-bottomed plates, were centrifuged, and were allowed to grow to reported size before initiation of treatment (*6*). Spheroids were incubated with fluorescently labeled liposomes or antibody for 6 and/or 24 hours, respectively, to scale with their corresponding blood circulation times. As described in the Supplemental Information (*8*), at different times spheroids were sampled, sliced and the equatorial section was imaged using fluorescence microscopy. The spatial profiles (radial concentrations) were evaluated by employing an inhouse eroding code to determine the average fluorescence intensity of each 5μm concentric ring on the spheroids' sections. The spatial distributions at each time point were integrated (using the trapezoid rule) to evaluate the time-integrated-concentration(s) vs. radius.

Spheroid Growth and Outgrowth Studies

Spheroids were incubated for 6 hours with ^{225}Ac-DOTA-loaded liposomes (1mM total lipid) and/or 24 hours with ^{225}Ac-DOTA-SCN-trastuzumab (10μg/mL). Upon completion of incubation, spheroids were transferred to fresh media and the spheroid volume was monitored until the non-treated spheroids stopped growing (17 days later) at which point spheroids were individually plated on cell culture-treated, flat-bottom 96-well plates and were allowed to grow. The number of live cells per well was reported as % outgrowth relative to the numbers of live cells that received no treatment, when the latter reached confluency.

Animal Studies

One million BT474 cells suspended in 100μl of 50:50 v:v Matrigel™:serum-free Hybricare media were inoculated into the second mammary fat pad of 5-to-6 week old NCR-nu/nu female mice (Taconic, Germantown, NY) at 24 hours following subcutaneous implantation of a 17β-estradiol (1.7mg)+progesterone (10mg) hormone pellet (Innovative Research of America, Sarasota, FL).

Upon tumors reaching 50mm^3, mice were randomly assigned to a group. For biodistribution studies, animals were I.V. administered (352-444kBq per animal) of ^{111}In-DTPA-encapsulating liposomes or ^{111}In-DTPA-SCN-trastuzumab in 0.1mL, and at different time points, animals were sacrificed, and organs were weighed and measured for radioactivity.

In addition to the cold conditions and to no treatment, for treatment studies, mice were administered I.V. a single 0.1mL injection of 4.625kBq or 9.25kBq of ^{225}Ac-DOTA-SCN-trastuzumab, ^{225}Ac-DOTA-loaded liposomes, or a combination of the two at constant total administered radioactivity. The total mass of antibody was kept constant at 15μg/mouse. Every other day, mice were weighed, and tumor volumes were measured with a digital caliper (resolution 0.01mm). Histopathology analysis was performed on H&E stained sections of all organs and tumors on day 24 after initiation of therapy.

α-Camera Imaging

Tumor-bearing mice were injected I.V. with ^{225}Ac-DOTA-SCN-trastuzumab, ^{225}Ac-DOTA-loaded liposomes or both at 148kBq total radioactivity and were sacrificed 24 hours later. Tumor and tissues were immediately harvested and sliced. The exposure time for the α-Camera was 24 hours per sample (*10*), and the images were analyzed using ImageJ 1.49b (NIH, Bethesda, MD) after being decay-corrected to the time of sacrifice.

MRI Imaging for Evaluation of Tumor pH_e

Briefly, animals were injected I.P. with the pH_e probe [(±)2-(imidazol-1-yl)succinic acid] (ISUCA), and anatomical T2 weighted spin-echo images were acquired using Rapid Acquisition Relaxation Enhancement (RARE) sequence on a Bruker BioSpec 9.4 T horizontal MR scanner. pH_e was determined as described in detail in the Supplemental Information (*11*).

Dosimetry

Dosimetry was performed following the methodology described in references (*12,13*) using the software package 3D-RD-S, Radiopharmaceutical Imaging and Dosimetry, LLC (Rapid, Baltimore MD) based on the biodistributions (1) of ^{111}In-labeled liposomes (Supplemental Tables 1, 2, Supplemental Fig. 1), and/or (2) of the radiolabeled antibody (as described in detail in reference (*14*)). ^{111}In has been confirmed as a surrogate of ^{225}Ac biodistribution ((*14*) and Supplemental Fig. 2). The longest-lived ^{225}Ac daughter, Bismuth-213, for the non-cell-internalizing liposomes, unlike for the cell-interalizing trastuzumab, was estimated to partly (25%) translocate from the site of the original parent decay (*13*).

Statistical Analysis

Results are reported as the arithmetic mean of n independent measurements ± the standard deviation. Significance in multiple comparisons and pair comparisons was evaluated by one-way ANOVA and unpaired Student's t-test, respectively, with *p*-values 0.05 considered to be significant.

RESULTS

Carrier Characterization

Table 1 shows the change of liposomes' apparent zeta potential with lowering pH towards less negative values; this was partly attributed to the protonation of DAP, on the 'adhesion lipid', with apparent pKa of 6.8 (*8*). Acidification also resulted in release of encapsulated ^{225}Ac-DOTA from liposomes (Supplemental Fig. 3). Characterization of the radiolabeled trastuzumab is summarized in Table 2 (and Supplemental Fig. 4).

Survival Assay on Cell Monolayers

Both cell lines, in monolayers, exhibited same sensitivity to free ^{225}Ac-DOTA and to ^{225}Ac-DOTA-encapsulating liposomes, independent of pH (Fig. 1 and Supplemental Fig. 5), since liposomes were designed to minimally associate with cancer cells (*8*) as is also the case for free ^{225}Ac-DOTA. Both cell lines exhibited comparable survival responses to ^{225}Ac-DOTA-SCN-trastuzumab demonstrating lack of resistance to α-particles independent of the reported resistance to trastuzumab for BT474-R. The HER2 expression by the two cell lines was comparable ($1.5x10^6$ vs $0.93x10^6$ copies per cell, Supplemental Fig. 4).

Spheroids: Spatiotemporal Microdistributions and Response to Delivered ^{225}Ac

The time integrated microdistributions of trastuzumab in spheroids (Fig. 2A), used as surrogates of tumor avascular regions, exhibited high accumulation only within the first 60μm from the spheroid edge with less than 10% of the peak value at distances beyond 100μm from the edge (indicated by a horizontal bracket). As expected, liposomes did not penetrate the spheroids longer distances than the antibody (Fig. 2B). Conversely, at distances 80μm from the spheroid edge and beyond, the fluorophore (Fig. 2C), that was used as a drug surrogate and was released from the liposomes, exhibited uniform time-integrated values at approximately 25% of its peak value (indicated by a horizontal bracket). However, close to the

spheroid edge, the released fluorophore cleared too fast from the spheroid (indicated by the vertical bracket). The acidification of the spheroids' interstitial pH (pH_e), which triggers the properties of liposomes' adhesion and content release, ranged from 7.4 close to the spheroids' edge to around 6.5 at the spheroid center (Supplemental Fig. 6). The time-integrated microdistributions on Fig. 2 reflect microdosimetry of the delivered ^{225}Ac but not of the radioactive daughters.

Following exposure to ^{225}Ac, divided between liposomes and the antibody, the carrier(s) resulting in greatest suppression of spheroid outgrowth depended on the spheroid size at the time of treatment. On small spheroids (100μm-radius), delivery of radioactivity by the targeting antibody (Fig. 2D) was most efficient. The heterogenous distribution of trastuzumab (high uptake but mostly localized close to the spheroid edge, Fig. 2A) did not impact efficacy because the longest spheroid distance (100μm-radius) was comparable to the range of α-particles in tissue (≤100μm) (*6*). On large spheroids (300μm-radius, corresponding to avascular distances almost 3 times longer than the range of α-particles in tissue) delivery of radioactivity by liposomes, that released in the interstitium ^{225}Ac-DOTA, was most efficient; this was attributed to the deeper penetration (as supported by the fluorescent surrogate in Fig. 2C) of released ^{225}Ac-DOTA toward the spheroid center (*6*). In spheroids with intermediate size (200μm-radius), the combination of the two carriers resulted in better cell kill.

Tumor/Tissue pH_e Measurement

The MRI images in Fig. 3 showed (1) that there was measurable acidity in the tumor interstitium, and (2) that the microdistributions of intertitial pH_e tumor maps were not uniform; indeed, they varied across tumors from different animals. Importantly, the pH_e values measured were close to the acidic values that trigger the release and adhesion properties on liposomes.

***In Vivo* Assessment**

In agreement with the profiles of delivered microdistributions of therapeutics in spheroids (Fig. 2), the tumor microdistributions of radioactivity *in vivo* were more uniform when delivered by both carriers compared to each carrier alone. In particular, the *normalized* microdistributions of ^{225}Ac in tumor sections, were more heterogeneous when the entire radioactivity was delivered by each carrier alone (Figs. 4A and 4B, top panel) compared to the simultaneous delivery of the same total radioactivity that was split between the two carriers (Fig. 4C). The top panel shows the normalized tumor microdistributions (where each pixel intensity was divided by the average of the intensities over the entire tumor section), and areas colored in red (ratio equal to 1) indicated local values closer to the mean tumor-delivered radioactivities. Importantly, in both tumor sections where ^{225}Ac was delivered only by a single carrier, the cyan and deep blue colored regions occupied significant area fractions; dark blue regions indicated local delivered radioactivities well-below the mean tumor-delivered values and, therefore, could result in lower cell kill. In densely vascularized areas (CD31-positive areas, green inserts) the delivered normalized radioactivity levels were closer to and above unity (unity = red; colors ranged from red to purple), whereas in sparsely vascularized areas (yellow inserts) colors ranged from deep blue (for the antibody, B) to cyan (for liposomes, A) to light red (for the combination, C).

In agreement with the extent of uniformity in tumor microdistributions of ^{225}Ac, the greatest inhibition of the volume growth of orthotopic BT474 xenografts was observed when radioactivity was delivered by equally splitting the same total radioactivity (9.25kBq (*6*)) between the two carriers (4.62kBq+4.62kBq) that were administered simultaneously (half-black-half-white circles); this is to be contrasted to administering the same total radioactivity (9.25kBq) by each carrier alone (*p*-values<0.001, Fig. 5A).

Notably, based on the dosimetry on Table 3, the equal radioactivity split between the two carriers that resulted in best tumor inhibition, delivered less dose at the tumor than when the antibody alone was used, underscoring the significance of α-particle *microdistributions* within the tumors. Individual animal tumor growth plots are shown in Supplemental Fig. 7. The same trend was observed at half the total

administered radioactivity (Supplemental Figs. 8 and 9). Table 3 also shows that the carrier combination delivered less dose at the kidneys than the antibody alone. The delivered dose at the liver by the carrier combination was similar to the dose delivered by each carrier alone. The error on the calculated dose to the spleen, delivered by the radiolabeled antibody, was large due to poor fitting. For more accurate fitting for the dose calculation to the spleen, sampling at longer time points would be required, to capture the biological clearance from the spleen.

Pathology evaluation of tumors on day 24 demonstrated visibly increased collagen upon treatment with ^{225}Ac when delivered by the combination of both carriers compared to each carrier alone (Fig. 5B). Histopathology analysis showed no noteworthy hepatic, cardiac, or renal toxicities across all constructs at the time of sacrifice (Supplemental Fig. 10). Slight inflammation in the diaphragm of the liposome-only treatment group was observed, but otherwise there was no visible lung inflammation. Additionally, increased cell death in and reduced size of the spleen was observed in the liposome-only condition, in agreement with their significant splenic uptake. Long-term renal toxicities (9.5 months post I.V. injection) of liposomal ^{225}Ac-DOTA at the maximum tolerated dose on tumor-free mice were not detected (*13*). The animal weight during the study did not decrease below 10% of the weight at the initiation of treatment (Supplemental Fig. 11).

Survival was not a meaningful end point in this study, because tumor growth was estrogen dependent; tumor growth rates (as shown by the non-treated group, Fig. 5A) reached an asymptote after approximately 60 days from estrogen pellet implantation.

DISCUSSION

We hypothesized that improvement of the spatial uniformity of an α-particle emitter within solid tumors may address the challenge of partial irradiation by α-particles and, therefore, improve efficacy even at lower tumor absorbed doses. In this study we demonstrated, using a simple and clinically implementable approach, that improvement of the spatial intratumoral uniformity of ^{225}Ac can be enabled by combinations of two separate carriers with complementary tumor microdistributions. Our approach optimized payload delivery; delivering a large number of α-particles at the tumor *perivascular regions* (via the targeting antibody) where the cell number is greatest and where cells are growing most aggressively, and, simultaneously, a high capacity penetrating payload to the tumor *interior* (via the tumor-responsive liposomes) where the dormant and resistant cells are most likely to be responsible for treatment failure (*15*). In the present study the same total administered radioactivity was equally divided between the two carriers resulting in synergistic inhibition of tumor growth compared to each carrier alone. It is possible that different radioactivity split ratios between the carriers may result in even better tumor growth inhibition solely due to more uniform spatiotemporal microdistributions of emitters within tumors.

In contrast to the (more) homogeneous microdistributions of the delivered radioactivity at the tumors, to improve killing of the cancer cell populations, the heterogeneous microdistributions, for example, at the liver, could explain the lack of hepatic toxicities on the basis of localized, partial irradiation. Although the liver uptake was significant when radioactivity was delivered by the liposomes, previous studies at the MTD with liposomes did not reveal any hepatic or splenic toxicities (the main off-target organs) even 9.5 months after injection (*13*). At least for the liver, one explanation for the fact that significant delivered doses *do not cause toxicities* may possibly be based on the *localized,* "*patchy" patterns of liver irradiation* (as opposed to the liver's uniform irradiation by the radiolabeled antibody). The hepatic delivered radioactivity by liposomes was strikingly "grainy", suggesting heterogeneous/partial irradiation and possibly limited cell kill (Supplemental Fig. 12). Liposomes are usually sequestrated by

Kupffer cells, that reside on the luminal side of the liver sinusoids, possibly limiting the irradiation to all hepatocytes. Hepatic toxicity was not observed in the present study where 63% of the MTD (*6*) was administered. Regarding the spleen, we have previously shown that at the MTD of ^{225}Ac delivered by liposomes, the initial splenic moderate-to-high hemosiderin deposition in the red pulp and reduced extramedullary hematopoiesis, observed right after administration of radioactivity, was found to subside and the spleen to fully recover after 9.5 months on tumor free mice (*13*).

Specific to ^{225}Ac are renal toxicities in mice which were previously partially connected to the escape in the blood of the last radioactive daughter of ^{225}Ac, Bismuth-213, when ^{225}Ac was delivered by long circulating carriers, such as antibodies, in addition to antibody renal uptake (*16*). For the ^{225}Ac-encapsulating liposomes, long-term renal toxicities at the MTD were not observed in mice (*13*). In human trials using ^{225}Ac-labeled antibodies or small molecules (*3,17*), renal toxicities have not been reported yet. For liposomes, it would most possibly be the hepatic and splenic uptake which could raise concerns possibly requiring further investigation (*18*).

In an effort to potentially mitigate toxicities at the liver and spleen by decreasing the corresponding delivered dose rates, radiolabeled antibodies were administered 72 hours after administration of radiolabeled liposomes. In spheroids, the order and lag time (up to 72 hours) of administering each of the carriers did not significantly affect the inhibition of spheroid outgrowth (Supplemental Fig. 13). In mice, this approach (Figure 5A, half-black half-grey symbols) still improved tumor growth inhibition relative to delivering the same total radioactivity by each carrier alone. Alternatively, a strategy that warrants investigation is dose fractionation of the antibody and/or liposome carriers, that may potentially provide therapeutic and toxicity advantages. Notably, the presented dosimetry assumed the biological clearance kinetics from tissues of the delivered radionuclides to be comparable to the half-life of ^{225}Ac. This assumption introduced an uncertainty in the calculated total

emitted energies retained by tissues in mice; it is possible that in humans the relative uncertainties are smaller, given that the clearance kinetics of carriers from tissues are known to be slower than in mice.

Two points are key to the clinical relevance and applicability of this approach; first is the vascular permeability of tumors to the administered liposomes; when human tumors exhibit vascular permeability to liposomes, then the extent of liposome uptake by tumors is strongly and favorably correlated with tumor response (*18*). Second is the acidification of the intratumoral pH_e as it relates to triggering the properties of adhesion and release on our liposomes; acidification is common on tumors of patients with breast (and other) cancers (*15*) and is correlated with highly aggressive tumors (*9,15,19*), with reported values comparable to the values, $6.60 \leq pH_e \leq 6.98$, required to activate our liposomes. Importantly, in our studies, although the intratumoral acidity was highly variant, the strategy of combining the two carriers still resulted in better tumor growth inhibition.

Our delivery approach is aimed at the spatial scale of the *avascular tumor regions*; these regions are bounded/defined by the *distances to the nearest blood vessels* within the tumors, and their order of magnitude ranges from a few tenths of micrometers up to possibly several hundredths of micrometers (*20*). The *distances to the nearest blood vessels* in tumors *are not of the order of magnitude of the macroscopic tumor sizes,* although they are expected to increase in larger tumors (*20*). From this perspective, the intratumoral microdistributions of α-particle emitters delivered by our strategy, would be driven by the distributions of the *distances to nearest blood vessels* within tumors and not directly by the macroscopic size of the tumor itself (*21*).

The spheroids studied herein demonstrated the different efficacy of each of the two delivery carriers as a function of these distances (Figure 2D-2F). Effective scale up of this approach to human tumors will depend not only on the lengths of the distances to nearest blood vessels (which should be

within reach by the released highly-diffusing forms of the α-particle emitters), but, importantly, by the extent of uptake and microdistributions of the radioactivity in off-target organs such as the liver. The potential for successful scale up of this approach to humans will be determined by our ability to optimize the radioactivity microdistributions to be as uniform as possible *within the tumor* (for maximum killing efficacy) and as heterogeneous as possible *within the off-target normal organs* (for minimum toxicities), as we show is the case of the mouse liver for the radioactivity delivered by liposomes (Supplemental Fig. 12).

CONCLUSION

In conclusion, the findings of this study show the potential to expand the impact of α-particle therapies to established solid tumors by choosing combinations of carriers based on the complementarity of the intratumoral microdistributions of the delivered α-particle emitters while maintaining the same administered radioactivities.

ACKNOWLEDGEMENTS

This work was partially supported by a grant from the Elsa U. Pardee Foundation, the American Cancer Society Research Scholar Grant RSG-12-044-01, the National Science Foundation grant CBET1510015, and the Under Armour-Innovation Award.

DISCLOSURE

No potential conflicts of interest relevant to this article exist.

KEY POINTS

QUESTION: Can the partial irradiation of solid tumors by α-particles, delivered with traditional radionuclide carriers, be rectified to improve efficacy?

PERTINENT FINDINGS: The partial irradiation of solid tumors by α-particle emitters can be rectified by combining carriers with complementary intratumoral microdistributions of the delivered α-particle emitters.

IMPLICATIONS FOR PATIENT CARE: Combination of separate carriers with complementary intratumoral microdistributions of α-particle emitters (^{225}Ac in this study) could be a general strategy to control solid tumor growth both in preclinical investigations and in the design of personalized, α-particle therapies for patients.

REFERENCES

1. American Cancer Society. Cancer Facts & Figures. 2021. American Cancer Society website. https://www.cancer.org/research/cancer-facts-statistics.html Accessed October 11, 2021

2. Kratochwil C, Bruchertseifer F, Giesel FL, et al. 225Ac-PSMA-617 for PSMA targeting alpha-radiation therapy of patients with metastatic castration-resistant prostate cancer. *J Nucl Med.* 2016;57:1941-1944.

3. Kratochwil C, Haberkorn U, Giesel FL. ^{225}Ac-PSMA-617 for Therapy of Prostate Cancer. *Semin Nucl Med.* 2020;50:133-140.

4. Yard BD, Gopal P, Bannik K, Siemeister G, Hagemann UB, Abazeed ME. Cellular and Genetic Determinants of the Sensitivity of Cancer to α-particle Irradiation. *Cancer Res.* 2019;79:5640-5651.

5. McDevitt MR, Sgouros G, Sofou S. Targeted and Nontargeted α-Particle Therapies. *Annu Rev Biomed Eng.* 2018;20:73-93.

6. Zhu C, Sempkowski M, Holleran T, et al. Alpha-particle radiotherapy: For large solid tumors diffusion trumps targeting. *Biomaterials.* 2017;130:67-75.

7. Wang R, Coderre JA. A Bystander Effect in Alpha-Particle Irradiations of Human Prostate Tumor Cells. *Radiat Res.* 2005;164:711-722.

8. Stras S, Howe A, Prasad A, Salerno D, Bhatavdekar O, Sofou S. Growth of Metastatic Triple-Negative Breast Cancer Is Inhibited by Deep Tumor-Penetrating and Slow Tumor-Clearing Chemotherapy: The Case of Tumor-Adhering Liposomes with Interstitial Drug Release. *Mol Pharm.* 2020;17:118-131.

9. Vaupel P, Kallinowski F, Okunieff P. Blood Flow, Oxygen and Nutrient Supply, and Metabolic Microenvironment of Human Tumors: A Review. *Cancer Res.* 1989;49:6449-6465.

10. Bäck T, Jacobsson L. The alpha-camera: a quantitative digital autoradiography technique using a charge-coupled device for ex vivo high-resolution bioimaging of alpha-particles. *J Nucl Med.* 2010;51:1616-1623.

11. Pacheco-Torres J, Mukherjee N, Walko M, et al. Image guided drug release from pH-sensitive Ion channel-functionalized stealth liposomes into an in vivo glioblastoma model. . *Nanomedicine* 2015;11:1345-1354.

12. Sgouros G, Roeske JC, McDevitt MR, et al. MIRD Pamphlet No. 22 (abridged): radiobiology and dosimetry of alpha-particle emitters for targeted radionuclide therapy. *J Nucl Med.* 2010;51:311-328.

13. Prasad A, Nair R, Bhatavdekar O, et al. Transport-oriented engineering of liposomes for delivery of α-particle radiotherapy: inhibition of solid tumor progression and onset delay of spontaneous metastases *Eur J Nucl Med Mol Imaging.* 2021;in press.

14. Song H, Hobbs RF, Vajravelu R, et al. Radioimmunotherapy of breast cancer metastases with alpha-particle emitter 225Ac: comparing efficacy with 213Bi and 90Y. *Cancer Res.* 2009;69:8941-8948.

15. Vaupel P. Tumor microenvironmental physiology and its implications for radiation oncology. *Semin Radiat Oncol.* 2004;14:198-206.

16. Song H, Hobbs RF, Vajravelu R, et al. Radioimmunotherapy of Breast Cancer Metastases with α-Particle Emitter ^{225}Ac: Comparing Efficacy with ^{213}Bi and ^{90}Y. *Cancer Res.* 2009;69:8941-8948.

17. Jurcic JG. Targeted Alpha-Particle Therapy for Hematologic Malignancies. *Semin Nucl Med.* 2020;50:152-161.

18. Lee H, Shields AF, Siegel BA, et al. ^{64}Cu-MM-302 Positron Emission Tomography Quantifies Variability of Enhanced Permeability and Retention of Nanoparticles in Relation to Treatment Response in Patients with Metastatic Breast Cancer. *Clin Cancer Res.* 2017;23:4190-4202.

19. Estrella V, Chen T, Lloyd M, et al. Acidity Generated by the Tumor Microenvironment Drives Local Invasion. *Cancer Res.* 2013;73:1524-1535.

20. Lauk S, Zietman A, Skates S, Fabian R, Suit HD. Comparative Morphometric Study of Tumor Vasculature in Human Squamous Cell Carcinomas and Their Xenotransplants in Athymic Nude Mice. *Cancer Res.* 1989;49:4557-4561.

21. Baish JW, Stylianopoulos T, Lanning RM, et al. Scaling rules for diffusive drug delivery in tumor and normal tissues. *Proc Natl Acad Sci USA.* 2011;108:1799-1803.

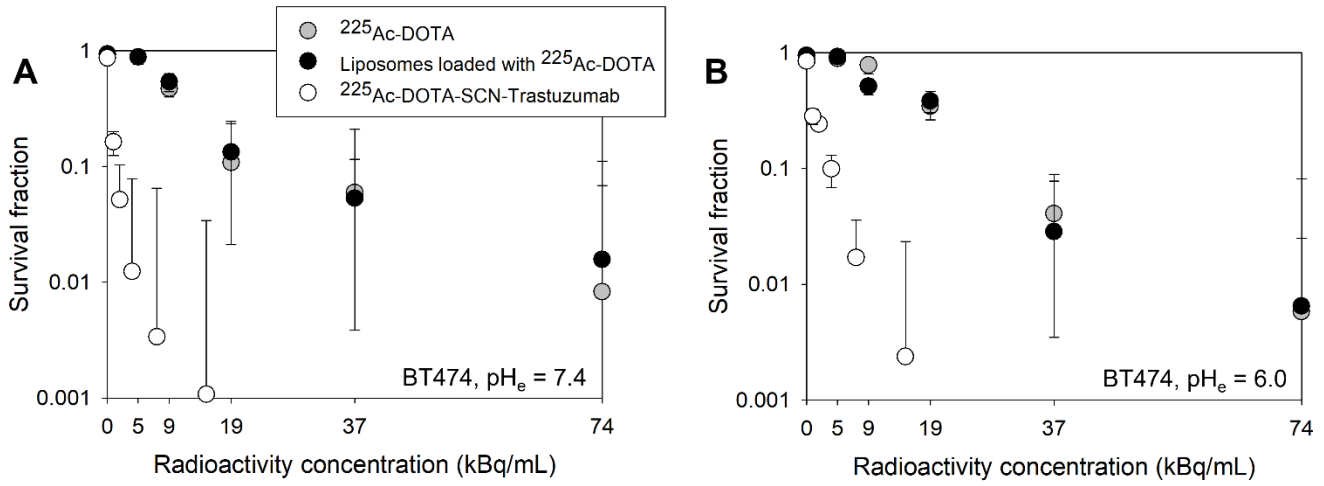

FIGURE 1. Colony survival of trastuzumab-sensitive BT474 (1.50±0.10 x 10^6 HER2 copies/cell) breast cancer cells following a 6 hour incubation at 37°C with free ^{225}Ac-DOTA (gray symbols), tumor-responsive liposomes loaded with ^{225}Ac-DOTA (black symbols) and radiolabeled trastuzumab (^{225}Ac-DOTA-SCN-Ab) (white symbols) at extracellular pH values of 7.4 (A) or 6.0 (B), as the lowest expected acidic value of the tumor interstitial pH_e. Radiolabeled trastuzumab's specific activity was 2.9MBq/mg at the highest radioactivity concentration. Cold conditions of liposomes and the antibody are indicated at zero radioactivity concentration. Error bars correspond to standard deviations of repeated measurements (4-6 samples per radioactivity concentration).

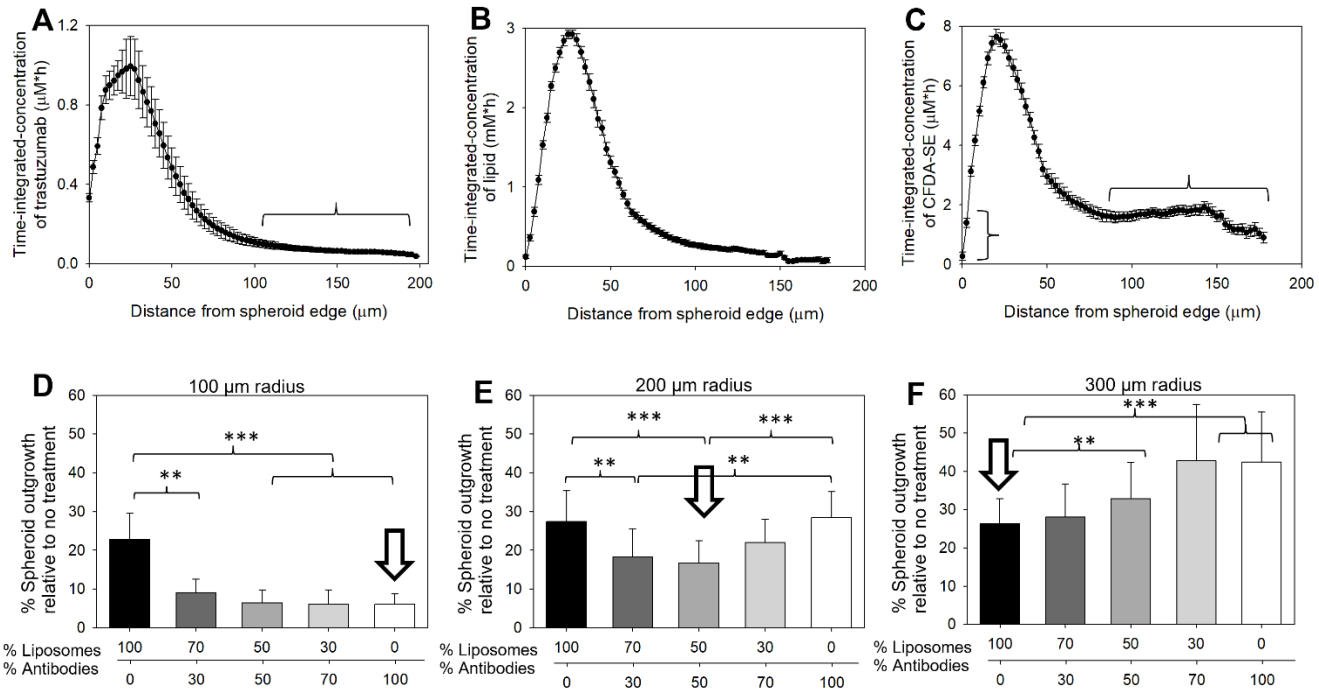

FIGURE 2A-C. Time-integrated concentrations in HER2-positive BT474 spheroids (r=200μm) of (A) the fluorescently labeled antibody (AlexaFluor-647-NHS-trastuzumab) used as surrogate of ^{225}Ac-DOTA-SCN-trastuzumab, (B) the lipids (DPPE-Rhodamine-labeled liposomes), and (C) the CFDA-SE fluorophores (used as surrogates of ^{225}Ac-DOTA) delivered by tumor-responsive liposomes. The spatial distributions obtained at different timepoints (during carrier uptake by and clearance from spheroids) were integrated using the trapezoid rule along the spheroid radius. Error bars correspond to the propagated standard deviations of the measurements of n=3-6 equatorial spheroid sections per time point. Immunoreactivity of the fluorescently-labeled antibody was: 88.2±2.7%.

FIGURE 2D-F. Greatest suppression of the extent of outgrowth (used as an indirect surrogate of tumor recurrence) by a carrier, or combinations of carriers, of ^{225}Ac depends on spheroid size (representing tumor avascular regions). Outgrowth control (D) of small spheroids (radius=100μm) was best enabled (indicated by arrow) by radiolabeled antibodies (^{225}Ac-DOTA-SCN-Trastuzumab), (F) of large spheroids (radius=300μm) by tumor-responsive liposomes encapsulating ^{225}Ac-DOTA, and (E) of medium size

spheroids (radius=200µm) by dividing the same total radioactivity between both carriers. The total radioactivity concentration was kept constant per spheroid size (D) 9.25kBq/mL, (E) 13.75kBq/mL, and (F) 18.5kBq/mL. Error bars correspond to the standard deviations of repeated measurements (n=4-5 spheroids per condition, 2 independent preparations). ** indicates 0.001<p-values<0.01; *** indicates p-values<0.001.

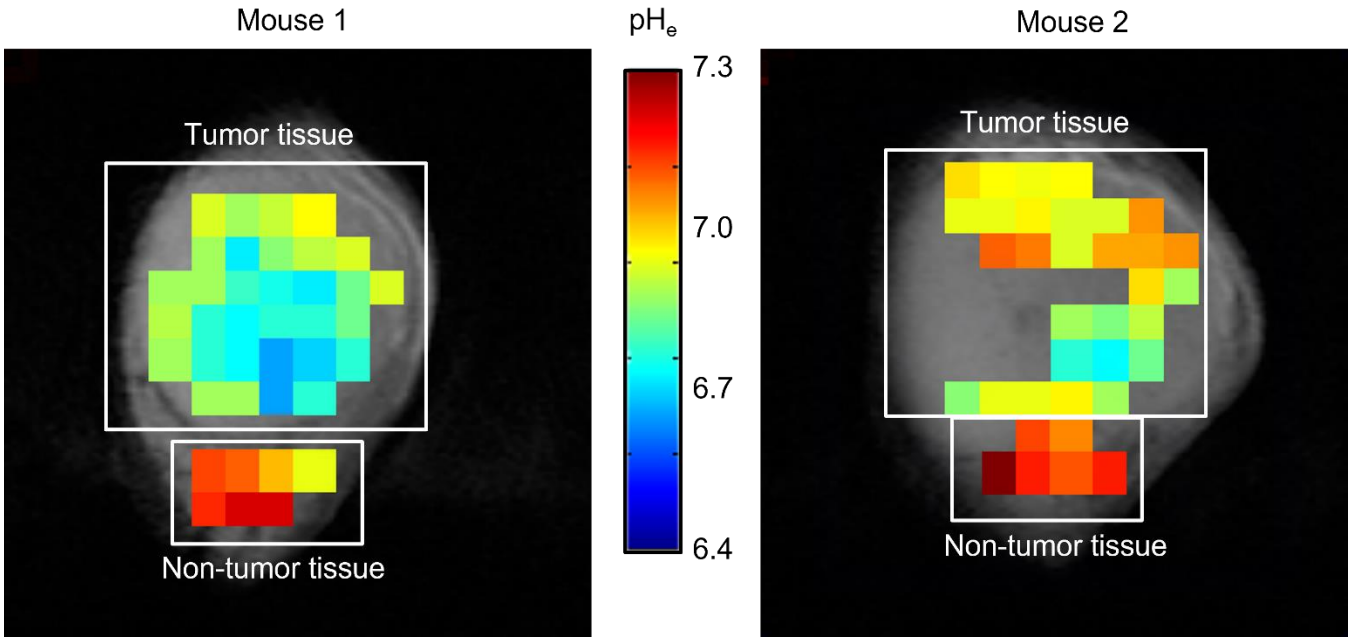

FIGURE 3. Tumor and non-tumor extracellular pH (pH_e) maps of two different animals with orthotopic BT474 xenografts on NCR nu/nu female mice which were administered I.P. with ISUCA, were imaged by MRSI. pH_e maps are presented overlaid with MRI anatomical images of the tumors. The ISUCA chemical shift for each voxel (1x1x4 mm^3) of the acquired multivoxel spectroscopy grid was transformed into a pH value using the Henderson-Hasselbalch calibration curve and presented as a colored pH_e map.

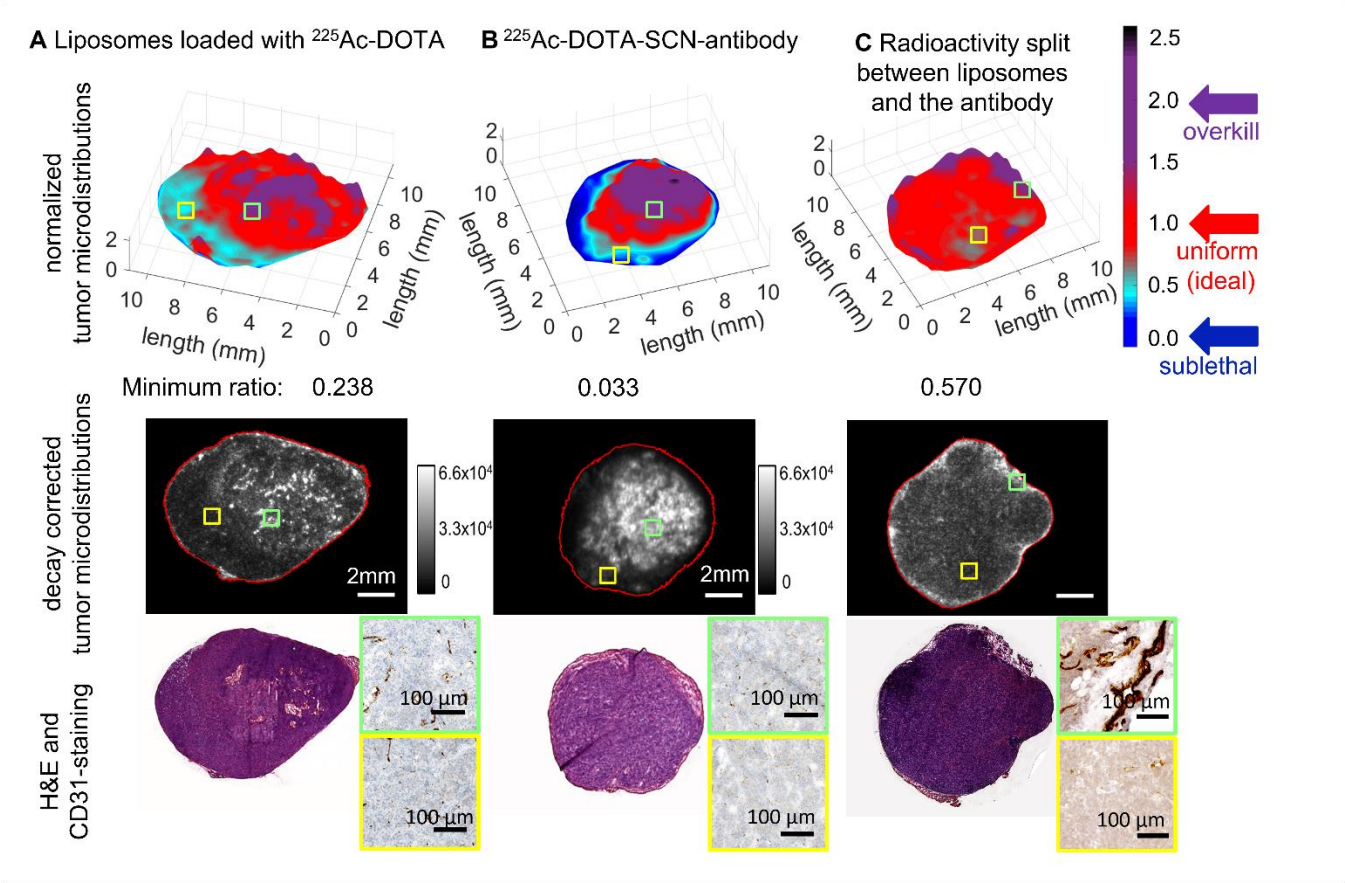

FIGURE 4. Microdistributions of the same total radioactivity of ^{225}Ac delivered by (A) tumor-responsive liposomes only, (B) the radiolabeled trastuzumab only, and (C) by both liposomes and the, separately administered, trastuzumab, on tumor sections harvested 24 hours post I.V. administration of 148kBq per animal. High radioactivity relative levels (ratios>2, purple) were detected in densely vascularized tumor areas (CD31+, indicated in green inserts); low radioactivity relative levels (ratios<0.6) were detected in sparsely vascularized areas (yellow inserts).

Top panel: Map of normalized pixel intensities (ratios) of ^{225}Ac relative to the mean value of intensities averaged over the entire tumor section, so as to evaluate the range of heterogeneities in ^{225}Ac-microdistributions. Regions in red (with ratios around unity) indicate local distributions close to the mean tumor-delivered radioactivities. Regions in cyan and dark-blue (with normalized pixel intensity ratios well-below the mean tumor-delivered radioactivities) indicate regions with low or too low radioactivities relative

to the tumor mean, expected to result in less cell kill. Regions in purple indicate areas where significantly more than the tumor-averaged radioactivity is delivered.

Middle and Bottom panels: Decay-corrected α-Camera images, and H&E-, and CD31- stained images of sequential 16 μm-thick-tumor sections.

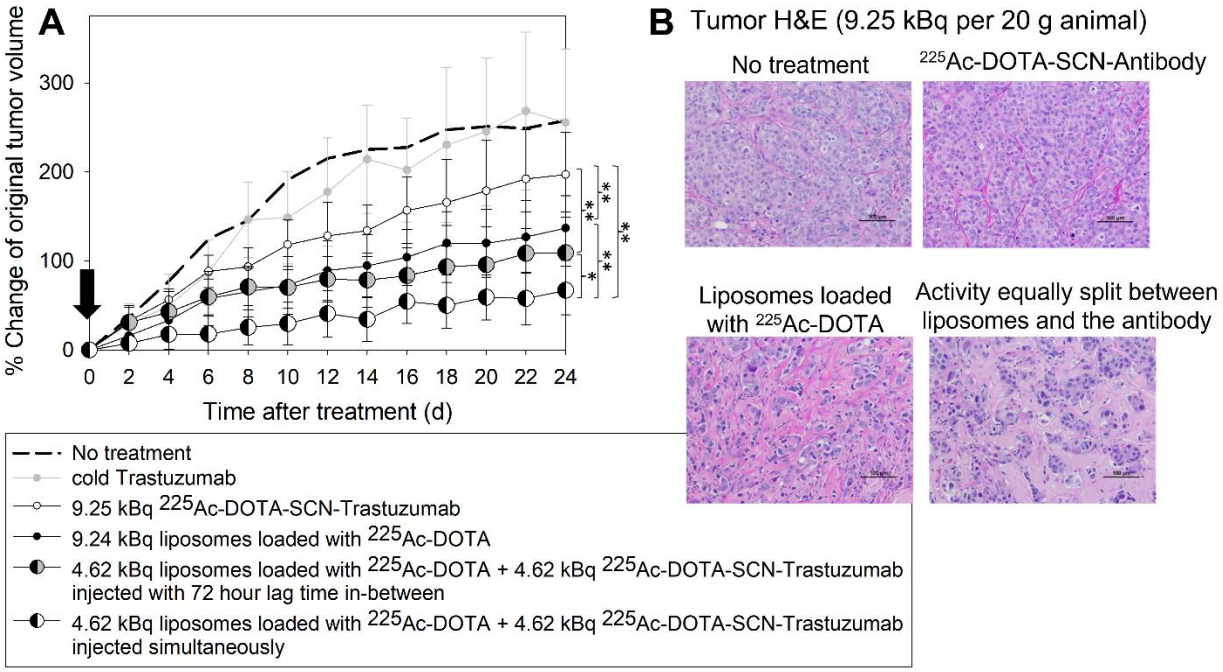

FIGURE 5. (A) Volume progression of HER2-positive BT474 orthotopic xenografts on NCR nu/nu female mice following a single I.V. administration (indicated by the black arrow) of 9.25kBq per 20g mouse of ^{225}Ac delivered by the radiolabeled trastuzumab alone (^{225}Ac-DOTA-SCN-antibody, 2.96 MBq/mg specific radioactivity in injectate) (white circles), the tumor-responsive liposomes loaded with ^{225}Ac-DOTA alone (black circles), by both carriers at equally split (same total) radioactivity with the radiolabeled antibody being administered 72 hours *after* the liposomes (to largely allow for the clearance of the latter from the liver and spleen) (half-black-half-gray circles), and by both carriers at equally split (same total) radioactivity injected simultaneously (half-black-half-white circles). Data points are the mean values and error bars the standard deviations of n=8–9 animals per group. Significance was calculated with one-way ANOVA (*p*-value<0.05). * indicates 0.01<*p*-values<0.05; **0.001<*p*-values<0.01.

(B) H&E stained tumor sections. Scale bar=100µm.

Graphical Abstract

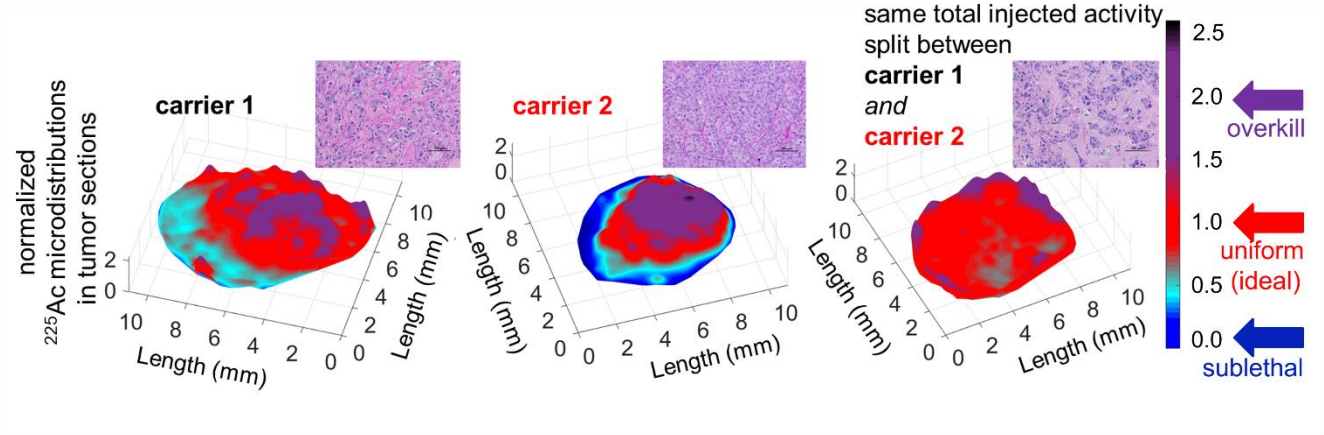

TABLE 1. Characterization of tumor-responsive liposomes loaded with ^{225}Ac-DOTA. * indicates 0.001<*p*-values<0.01, $^{\#}$*p*-values<0.001.

Size, nm (PDI)	Zeta Potential (mV)			% Loading	Specific activity (MBq/µmol lipid)	Retention Kinetics $y = y_\infty + a * e^{-bt}$				
	pH 7.4	pH 6.5	pH 6.0			pH	y_∞ (%)	a (%)	b (1/h)	t½ (h)
118 ± 15 (0.099 ± 0.051)	-1.5 ± 1.4*	-0.8 ± 1.2$^{\#}$	-0.04 ± 1.1$^{*, \#}$	51.1 ± 8.6	0.5 ± 0.2	7.4	88.8 ± 0.7	10.9 ± 1.2	1.2 ± 0.3	0.6 ± 0.2
						7.0	84.9 ± 1.3	13.8 ± 1.7	0.5 ± 0.1	1.4 ± 0.1
n = 15	n = 15	n = 15	n = 15	n = 15	n = 9 starting activity: 1.5 – 3.7 MBq	6.5	77.8 ± 1.2	21.2 ± 1.5	0.4 ± 0.1	1.7 ± 0.1
						6.0	72.4 ± 0.7	27.8 ± 1.0	0.7 ± 0.1	1.0 ± 0.0

TABLE 2. Characterization of ^{225}Ac-labeled HER2-targeting trastuzumab.

Radiolabeling efficiency %	Immunoreactivity %	Specific activity (MBq/mg Ab)	Radiochemical Purity	24 hour retention %	K_D (nM)	
					BT474	BT474-R
53.8 ± 11.4	95.9 ± 1.4	3.4 ± 0.7	97.8 ± 1.8	90.6 ± 2.5	24.6 ± 4.9	10.2 ± 1.7
n = 14	n = 14	n = 11 starting activity: 0.4 – 1.1 MBq	n = 14	n = 14		

TABLE 3. Dosimetry results.

Tissue	Absorbed dose (Gy)*					
	Antibody only		Liposomes only		Same total injected radioactivity equally split between the antibody and the liposomes	
	D	SD	D	SD	D	SD
Kidneys	6.25	0.79	0.17	0.07	3.21	0.79
Liver	2.21	1.21	1.08	0.22	1.64	1.23
Lungs	0.94	0.29	0.22	0.21	0.58	0.36
Spleen	9.51	30.60	1.41	0.54	5.46	30.60
Tumor	6.68	1.55	0.40	0.06	3.54	1.55

*mean and standard deviation (SD), not adjusted by relative biological effectiveness.

Supplemental Information

Materials

Lipids 1,2-diarachidoyl-sn-glycero-3-phosphocholine (20PC), 1,2-dipalmitoyl-sn-glycero-3-phospho-L-serine (sodium salt) (DPPS), 1,2-dipalmitoyl-sn-glycero-3-phosphoethanolamine-N-(Lissamine Rhodamine B Sulfonyl) (Ammonium Salt) (DPPE-Rhodamine), and 1,2-distearoyl-sn-glycero-3-phosphoethanolamine-N-[amino(polyethylene glycol)-2000](ammonium salt) (DSPE-PEG) were purchased from Avanti Polar lipids (Alabaster, AL). Cholesterol, Sepharose 4B, Sephadex G50, sodium bicarbonate, diethylenetriaminepentaacetic acid (DTPA), calcium ionophore A23187, 4-(2-hydroxyethyl)-1-piperazineethanesulfonic acid (HEPES), poly(2-hydroxyethyl methacrylate) (PolyHEMA), ascorbic acid, sodium carbonate, Trizma base, crystal violet, sucrose, Matrigel™ were purchased from Sigma-Aldrich Chemicals (Atlanta, GA). Phosphate buffered saline (PBS) was purchased from Quality Biological (Gaithersburg, MD). Dimethylformamide (DMF) was purchased from Avantor Performance Materials (Center valley, PA). Ethylenediaminetetraacetic acid, disodium salt dihydrate (EDTA), BCA protein assay, trypsin, penicillin-streptomycin, and 2-propanol (IPA) were purchased from Fisher Scientific (Pittsburgh, PA). Hybricare medium and the BT474 cell line were both obtained from ATCC. Fetal Bovine Serum (FBS) was obtained from Omega Scientific (Tarzana, CA).

Methods

Liposome formation and radiolabeling

Liposomes composed of 20PC:DPPS:cholesterol:DSPE-PEG-DAP:DPPE-Rhodamine at 0.61:0.26:0.04:0.09:0.001 mole ratio and encapsulating 12.5mM DOTA in Citric acid buffer (150mM, pH 5.0) were formed using the thin film hydration method (6). Briefly, lipids (5 μmoles) were dried in round bottom flasks, and the film was hydrated with 375 μL Citric acid buffer (150 mM, pH 5.0), DOTA (125 μL, 20 mg/mL) and ascorbic acid (15 μL, 0.8M) and annealed for two hours at a temperature above 75°C. For loading of ^{111}In, liposomes encapsulated 2mM DTPA and

0.12mM Ascorbic acid in PBS (300mOsm pH 7.6). Lipid suspensions were then extruded 21 times through two stacked polycarbonate membranes with pore sizes of 100 nm and were then passed through a Sepharose 4B column equilibrated with HEPES buffer (20 mM, pH 7.4, 300 mOsm) to remove unencapsulated DOTA (or DTPA).

Then, the sample was incubated with a mixture of ^{225}Ac (dissolved in 0.2 N HCl) or ^{111}In, 25 µL of calcium ionophore A23187 in ethanol at 15.6 mg/mL, and 25 µL of water. The liposomes were incubated at 75°C for 1 hour, after which, the sample was allowed to cool. Upon reaching room temperature, the liposomes were passed through a Sephadex G-50 column to remove unentrapped ^{225}Ac or ^{111}In. The loading yield was calculated from a ratio of the activities before and after the Sephadex G-50 column, after reaching secular equilibrium (for ^{225}Ac), using an automated γ-counter (Cobra II Auto-Gamma, Packard Instrument Co., Inc).

Antibody radiolabeling

Trastuzumab was labeled with ^{225}Ac (or ^{111}In) using the “one step” method, and all buffers were prepared using metal-free water (6). First DOTA-SCN was conjugated to the antibody; in particular, DOTA-SCN was dissolved in DMF at 10 mg/mL and added drop wise to 0.5 mg/mL ice cold antibody solution in 0.1 M sodium carbonate buffer at pH 9.0 to achieve a 40:1 chelator/antibody ratio (DTPA-SCN at 20 mg/mL in DMSO at a 15:1 chelator:antibody ratio for ^{111}In labeling). This reaction was left to continue overnight at room temperature on a plate shaker. Upon completion of the reaction, non-conjugated DOTA-SCN was separated from DOTA-SCN-Trastuzumab conjugates using a 10-DG size exclusion column equilibrated with 0.1M Tris buffer at pH 9.0. Similarly, non-conjugated DTPA-SCN was separated from DTPA-SCN-Trastuzumab using a 10-DG column equilibrated with 1M acetate buffer, pH 4.5. Final antibody concentration was confirmed using BCA Assay.

Actinium-225 dissolved in 0.2M HCl was added to at least 100 µg antibody in 500 µL of 0.1M Tris buffer at pH 9.0 (or 1M acetate buffer at pH 4.5 for ^{111}In) and was allowed to incubate for 1 hour at 37°C. Free/non-chelated ^{225}Ac was removed by the addition of 50 µL of 10 mM DTPA. After 5 minutes, the sample was purified by a 10-DG column equilibrated with PBS and 1mM EDTA at pH 7.4 (6).

Radiochemical purity of ^{225}Ac-DOTA-SCN-labeled antibody was assessed using iTLC. Briefly, a spot of ^{225}Ac-DOTA-SCN-antibody was added towards the bottom of a strip of filter paper and allowed to dry completely. The iTLC strip was then vertically placed in a beaker with 10 mM EDTA in water (mobile phase), ensuring that the spot was not below the fluid level (6). The immunoreactivity was evaluated by incubation for 1 hour, on ice, with BT474 cells at 100x excess of HER2 receptors in the presence and absence of blocking by the cold antibody. Stability of radiolabeling was assessed by measuring the retained activity of the antibody after incubation in cell culture media at 37°C for 24 hours. Unbound activity was separated using a 10-DG column equilibrated with PBS at pH 7.4.

Antibody labeling with fluorophores

Trastuzumab was labeled with Alexa Fluor 647 NHS Ester (ex 651 nm; em 672 nm) in a 5:1 dye to antibody molar ratio in accordance with Thermo Fisher. Briefly, 2 mg/ml of Trastuzumab in 0.1M sodium bicarbonate at pH 8.3 was incubated with Alexa 647 for 2 hours. Unlabeled Alexa Fluor 647 was separated from labeled antibody using a 10DG column equilibrated with PBS at pH 7.4.

Clonogenic survival

Cell monolayers of 500,000 cells/well were plated in 6-well plates and were allowed to adhere overnight. After incubation for 6 hours with varying concentrations of radioactivity, the

cells were washed, scraped and resuspended in media in 3 different densities, and were plated in dishes to grow until the untreated cells formed colonies of > 50 cells per colony. Colonies were stained and counted (6), and the survival fraction was determined by normalizing the counted number of treated colonies to the number of untreated colonies, accounting for the plating efficiency (6).

Spatiotemporal Profiles in Spheroids

Liposomes labeled with 1 mole% DPPE-Rhodamine (ex/em: 550/590 nm) were loaded with CFDA-SE (ex/em: 497/517nm; used as the hydrophilic drug surrogate) and incubated with spheroids at 5mM total lipid. Trastuzumab was labeled with AlexaFluor647 NHS Ester (ex/em: 651/672nm) as described in the Supporting Information, and was incubated with spheroids at 20μg/ml.

Spheroids were incubated with fluorescently-labeled liposomes and/or the antibody for 6 and/or 24 hours, respectively. At different time points during incubation and after being moved to wells with fresh media, spheroids were sampled, immediately frozen in cryochrome gel, cryosectioned in 20 μm-thickness slices, and the equatorial slices were imaged and analyzed using an eroding code. The spatial distributions at each time point were integrated (using the trapezoid rule) to evaluate the are-under-the-curve (AUC) for each position within the spheroids. Spheroids without treatment were frozen similarly and used as background. Calibration curves for the concentration of liposomes, CFDA-SE, and/or the fluorescently-labeled antibody were performed with known concentrations in a quartz cuvette of 20 μm optical pathlength using the same microscope.

An inhouse eroding code in Matlab was used to determine the average intensity of each 5 μm concentric ring of the spheroid, moving from the edge to the core of the spheroid.

MRI-based measurement of tumor pH_e (verbatim from SI of (13))

In vivo MRI images were acquired on a Bruker BioSpec 9.4 T horizontal MR scanner using a home-built solenoid coil placed around the subcutaneous tumors. Animals were anaesthetized by inhalation of 2% isoflurane in oxygen and maintained with 1.0 to 1.5% isoflurane during the experiment. Anesthetized animals were fixed with tape to the plexiglass animal-holder to minimize breathing-related motion. The physiological state of the animal was monitored throughout the MRI experiment using a pneumatic pillow sensor recording the respiratory rate of the animal, that was kept around 30-50 bpm. This setup was then positioned in the isocenter of the magnet.

Briefly, anatomical T2 weighted spin-echo images were acquired in the three orthogonal directions using Rapid Acquisition Relaxation Enhancement (RARE) sequence. The following parameters were used: repetition time (TR) = 2000 ms, echo time (TE) = 48 ms, RARE factor = 8, 1 averages, field of view (FOV) = 40 x 40 mm, acquisition matrix (Mtx) = 128 × 128; 156 × 156 μm^2 in plane resolution, slice thickness = 1 mm and 12 slices. These slices were used to localize the 4 mm thick ^1H magnetic resonance spectroscopic imaging (MRSI) coronal slice. MRSI was acquired using a chemical shift imaging (CSI) sequence following administration of 200 μl i.p. of the pHe probe [(±)2-(imidazol-1-yl)succinic acid] (ISUCA) at a dose of 3 mg/g. Acquisition parameters were: FOV = 16 × 16 mm, CSI matrix = 8 × 8 zero-filled to 16 × 16, (final in-plane resolution 1000 x 1000 μm^2), slice thickness = 4 mm, TR = 1000 ms, TE =48 ms and 16 repetitions acquired during 17.2 min. Water suppression was performed with a Variable Pulse Power and Optimized Relaxation Delays (VAPOR) sequence. An anatomical T2 weighted image was acquired with the same geometry than the MRSI to be used as a reference. The following parameter were used: RARE sequence, TR = 2000 ms, TE = 32 ms, RARE factor = 8, 1 averages, FOV = 16 x 16 mm, acquisition matrix (Mtx) = 128 × 128; 125 × 125 μm^2 in plane resolution, slice thickness = 4 mm.

pHe map analysis

MRSI images were reconstructed using 3DiCSI 1.9.9 software (Hatch Center for MR Research, Columbia University, New York, NY). pHe maps were obtained as previously described (11). In the presence of ISUCA, Lorentzian line shapes were fitted to the H2 peaks to obtain the H2 chemical shifts using the endogenous choline resonance as reference (3.21 ppm). Only those voxels with signal-to-noise ratio (SNR) higher than two were considered. Extracellular pH was then determined in each voxel from the chemical shift of the H2 peak using the Henderson-Hasselbalch equation:

$$pH = pk_a - log\frac{\delta_1 - \delta}{\delta - \delta_2}$$

where, pk_a = 7.07, δ is the measured ISUCA H2 chemical shift and δ1 (8.75) and δ2 (7.68) are the alkaline and acidic asymptotic values of the ISUCA titration curve.

	^{111}In-DTPA-SCN-Trastuzumab				
	% IA/g				
	Time points (hours)				
	1	**8**	**24**	**48**	**72**
Heart	5.15 ± 1.75	2.19 ± 0.90	2.39 ± 0.78	1.95 ± 0.80	1.72 ± 1.06
Lung	6.87 ± 2.08	7.30 ± 3.79	3.64 ± 1.05	5.42 ± 0.73	3.11 ± 1.20
Liver	10.47 ± 4.73	10.34 ± 2.89	8.52 ± 3.36	9.87 ± 2.22	7.33 ± 3.42
Spleen	4.15 ± 1.29	8.44 ± 4.25	12.16 ± 2.00	16.40 ± 3.95	16.67 ± 2.54
Kidney	8.07 ± 1.99	6.87 ± 1.53	9.26 ± 2.35	10.32 ± 2.81	13.83 ± 3.43
Stomach	2.10 ± 0.68	2.52 ± 0.18	1.47 ± 0.29	2.35 ± 0.82	1.47 ± 0.08
Intestine	2.08 ± 1.90	3.17 ± 0.15	1.52 ± 0.88	2.35 ± 1.38	2.26 ± 0.79
Bone	0.22 ± 0.56	1.07 ± 0.29	0.77 ± 0.31	1.52 ± 0.31	1.22 ± 0.51
Muscle	1.31 ± 0.83	0.69 ± 0.35	1.21 ± 0.89	0.61 ± 0.14	0.91 ± 0.53
Blood	14.52 ± 4.34	7.12 ± 2.99	4.77 ± 1.98	2.99 ± 1.43	3.22 ± 0.41
Tumor	0.78 ± 0.32	5.64 ± 5.31	8.07 ± 3.07	10.39 ± 4.69	15.40 ± 6.89

SUPPLEMENTAL TABLE 1. **Biodistributions in mice** bearing orthotopic BT474 xenografts of I.V. administered ^{111}In-DTPA-SCN-trastuzumab used as surrogate of ^{225}Ac-DOTA-SCN-trastuzumab. Error bars correspond to standard deviations of measurements averaged over n=3 mice per time point.

	^{111}In-DTPA-encapsulating liposomes				
	% IA/g				
	Time points (hours)				
	1	**16**	**24**	**32**	**48**
Heart	3.61 ± 1.43	1.37 ± 0.55	1.45 ± 1.40	0.88 ± 0.53	0.46 ± 0.15
Lung	2.32 ± 1.56	0.66 ± 0.17	0.86 ± 0.21	0.63 ± 0.32	0.48 ± 0.32
Liver	7.67 ± 3.71	5.36 ± 1.13	9.66 ± 1.39	5.85 ± 2.42	4.52 ± 1.78
Spleen	1.41 ± 0.88	4.60 ± 1.93	6.62 ± 1.82	13.44 ± 5.12	8.14 ± 3.11
Kidney	1.63 ± 1.49	0.63 ± 0.20	0.65 ± 0.47	1.46 ± 1.13	0.78 ± 0.43
Stomach	0.71 ± 0.61	0.50 ± 0.28	0.59 ± 0.46	0.21 ± 0.08	0.61 ±0.83
Intestine	0.40 ± 0.25	0.25 ± 0.09	0.18 ± 0.07	0.13 ± .016	0.08 ± 0.12
Bone	0.54 ± 0.43	1.00 ± 0.91	1.17 ± 1.63	0.20 ± 0.06	0.17 ± 0.12
Muscle	0.29 ± 0.13	1.07 ± 1.01	0.31 ± 0.35	0.19 ± 0.04	0.38 ± 0.32
Blood	19.10 ± 1.57	5.50 ± 1.33	2.52 ± 1.68	2.24 ± 1.32	0.48 ± 0.59
Tumor	0.94 ± 0.48	3.48 ± 1.30	5.34 ± 2.03	2.38 ± 0.78	1.48 ± 0.48

SUPPLEMENTAL TABLE 2. **Biodistributions in mice** bearing orthotopic BT474 xenografts of I.V. administered tumor-responsive liposomes encapsulating ^{111}In-DTPA, used as surrogate of ^{225}Ac-DOTA. Error bars correspond to standard deviations of measurements averaged over n=3 mice per time point.

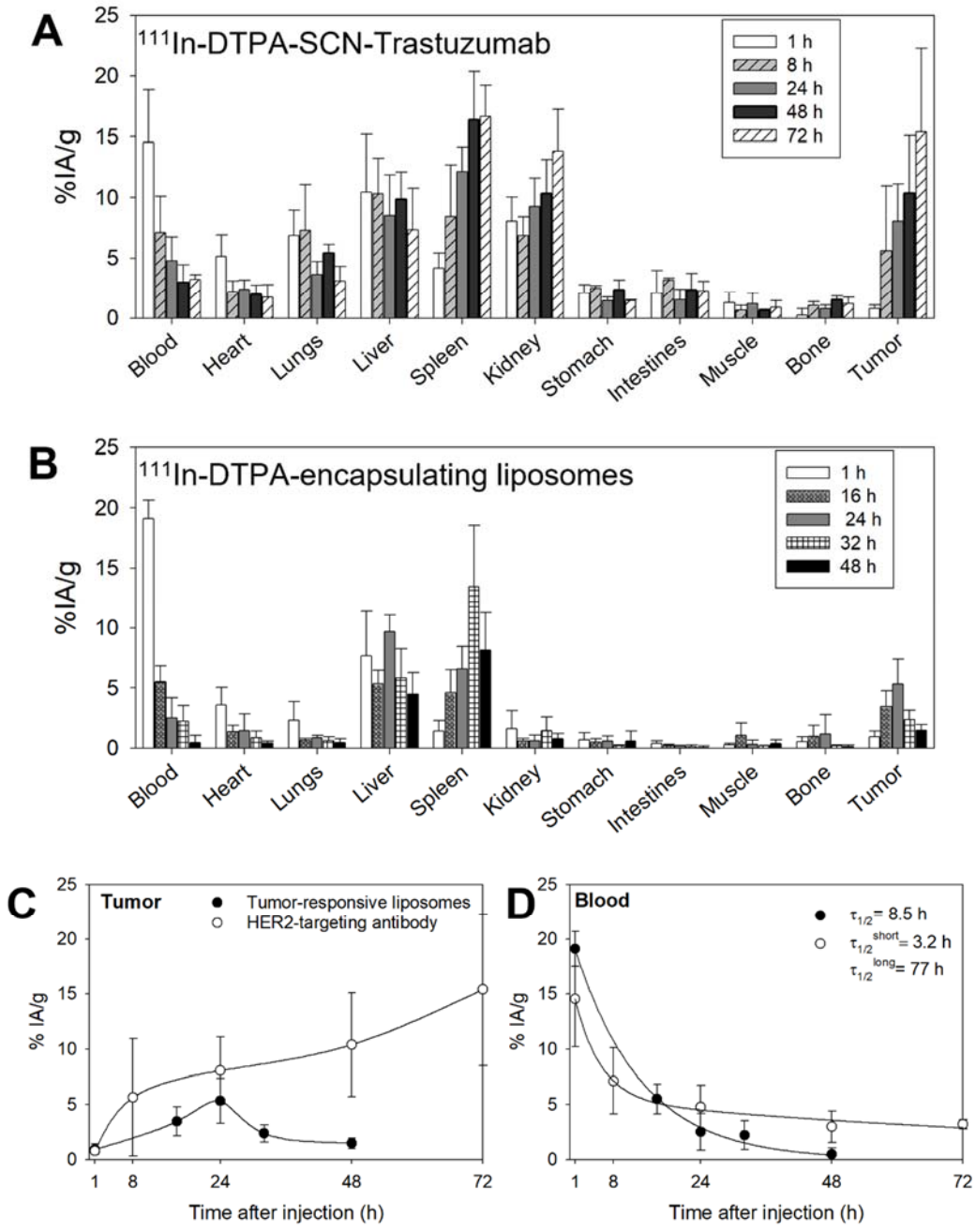

SUPPLEMENTAL FIGURE 1. Biodistributions in mice bearing orthotopic BT474 xenografts of I.V. administered (A) ^{111}In-DTPA-SCN-Trastuzumab and (B) tumor-responsive liposomes encapsulating ^{111}In-DTPA. (C) Comparison of blood clearance and tumor uptake/clearance of

each carrier. Error bars correspond to standard deviations of measurements averaged over n=3 mice per time point.

Radiolabeling stability of *t*rastuzumab with ^{111}In (89.3±4.4%, 24-hour radioactivity retention) and retention of ^{111}In-DTPA by liposomes was similar to trastuzumab radiolabeling with ^{225}Ac and to retention of ^{225}Ac-DOTA by liposomes, respectively (Tables 1 and 2 in main text, Supplemental Figure 2 *(13)*).

The biodistributions demonstrated the significantly greater mean tumor uptake of injected radioactivity when delivered by trastuzumab compared to the tumor uptake when radioactivity was delivered by liposomes (Supplemental Fig. 1C). ^{111}In has been confirmed as a surrogate of ^{225}Ac biodistribution (14). In liposomes, the same retention of ^{111}In and ^{225}Ac by tumor-responsive liposomes (Supplemental Fig. 2), justified the use of ^{111}In as surrogate of ^{225}Ac (13).

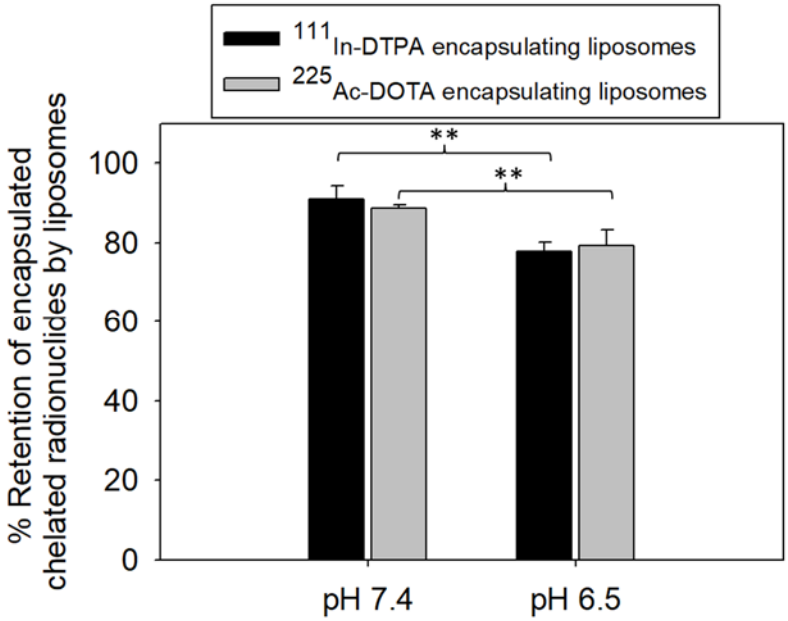

SUPPLEMENTAL FIGURE 2. Comparison of the retention of encapsulated ^{111}In-DTPA (black bars) and ^{225}Ac-DOTA (gray bars) by liposomes at neutral pH (left), and at acidic pH values (right) six hours post incubation at the corresponding pH conditions, at 37^{o}C. Errors correspond to standard deviations of n=3 independent liposome preparations. ** *p*-value < 0.05.

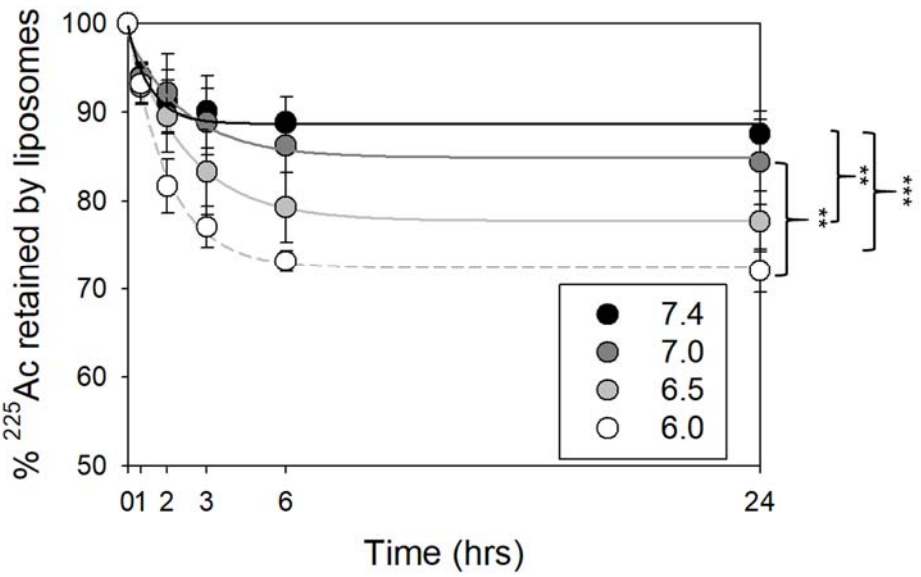

SUPPLEMENTAL FIGURE 3. **Kinetics of increasing release of ^{225}Ac from liposomes with lowering pH**. Liposomes were incubated in serum supplemented media (in the presence of cells) at 37^{o}C. At different time points, samples from the parent suspension were run through a size exclusion chromatography column to separate liposome-encapsulated radioactivity from released radioactivity, and the γ-emissions of Bismuth-213, the last radioactive daughter of ^{225}Ac, were counted after separated fractions reached secular equilibrium. The fitted kinetic constants are listed on Table 1 (main text). Errors correspond to standard deviations of n=4 independent liposome preparations. ** indicates 0.01< *p*-values < 0.05; *** indicates *p*-values ≤0.001.

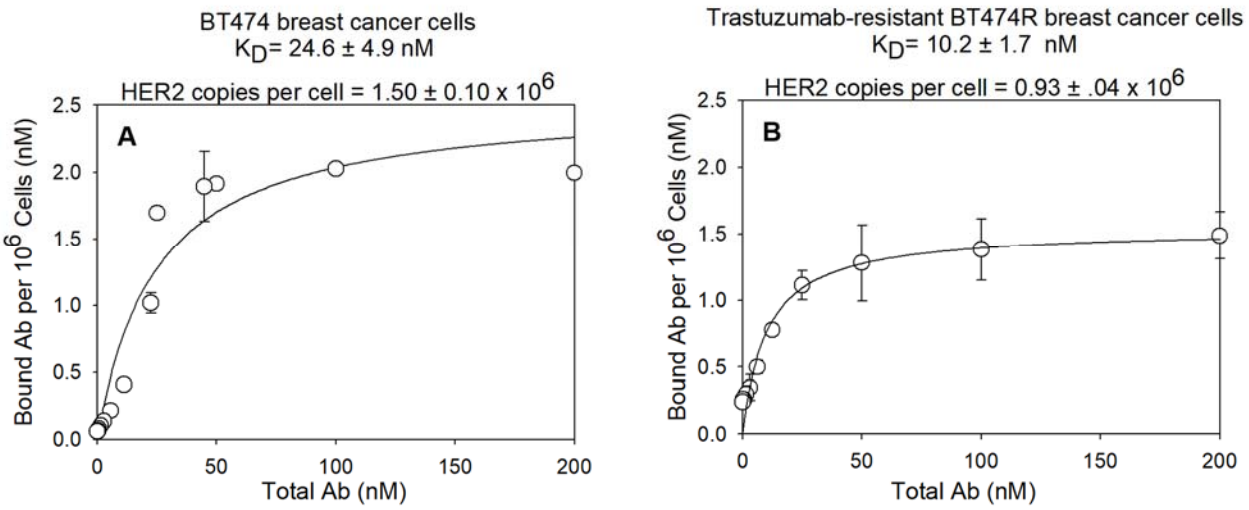

SUPPLEMENTAL FIGURE 4. **Binding curves of ^{111}In-DTPA-SCN-trastuzumab** with **(A)** the BT474 breast cancer cells and **(B)** the Trastuzumab-resistant BT474-R breast cancer cells. Immunoreactivity of the radiolabeled antibody was: 90.4 ± 5.3 %. All measurements were collected from suspended cells at a fixed concentration and maintained, constantly shaking, at ice-cold temperatures. Ab stands for antibody in above plots. Error bars correspond to standard deviations of repeated measurements (2 samples per preparation, 2 separate preparations).

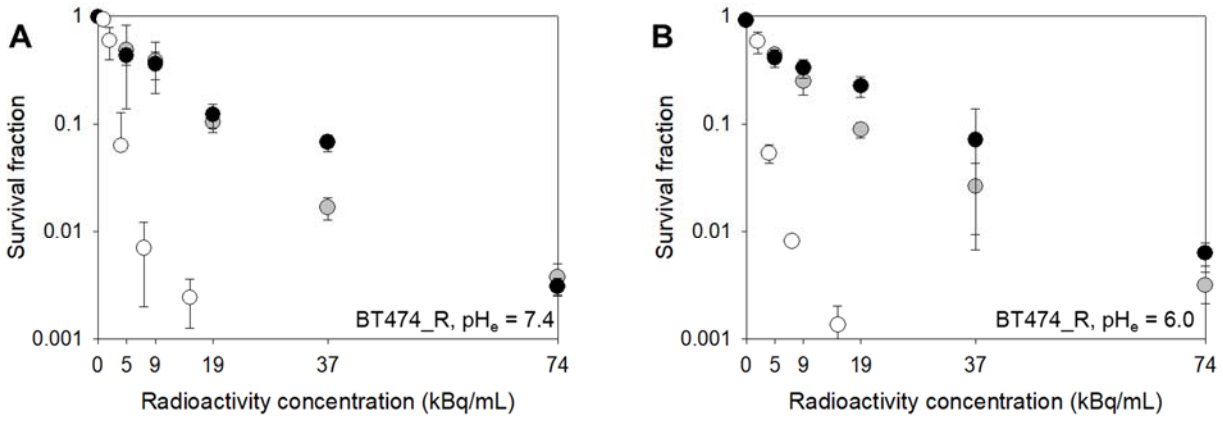

SUPPLEMENTAL FIGURE 5. Colony survival of trastuzumab-resistant BT474-R (0.93±0.04 x 10^6 HER2 copies/cell) breast cancer cells following a 6 hour incubation at 37°C with free ^{225}Ac-DOTA (gray symbols), tumor-responsive liposomes loaded with ^{225}Ac-DOTA (black symbols) and radiolabeled trastuzumab (^{225}Ac-DOTA-SCN-Ab) (white symbols) at extracellular pH values of 7.4 (A) or 6.0 (B), as the lowest expected acidic value of the tumor interstitial pH_e. Radiolabeled trastuzumab's specific activity was 2.9MBq/mg at the highest radioactivity concentration. Cold conditions of liposomes and the antibody are indicated at zero radioactivity concentration. Error bars correspond to standard deviations of repeated measurements (4-6 samples per radioactivity concentration).

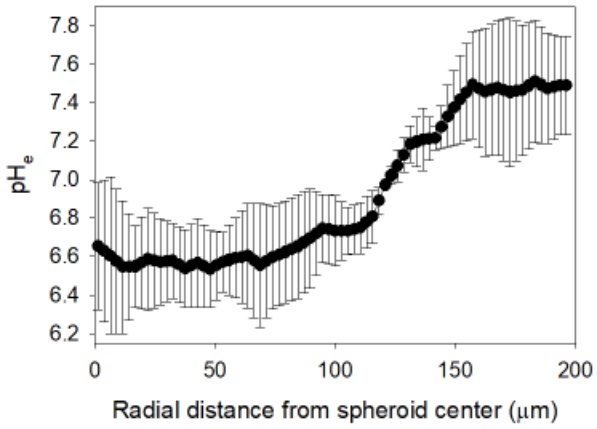

SUPPLEMENTAL FIGURE 6. Radial profile of the interstitial pH (pH_e) in BT474 spheroids of 400μm in diameter. The mean pH_e at the spheroid edge (r=200μm) ranged from 7.42 to 7.46, and the pH close to the spheroid center (r=0) was approximately 6.5.

Method for pH_e profile measurement

The pH_e of the interstitium of multicellular 400 μm-in-diameter spheroids as a function of spheroid radius was measured by incubating spheroids with 350μM solution of the membrane impermeant pH-indicator SNARF-4F in media overnight at 37°C. The ratio of SNARF-4F's emission intensities at 640 nm and 580 nm (ex: 514 nm) varies linearly with pH between the values 6 to 8 independent of the fluorophore's concentration. Right before using a Zeiss LSM 780 confocal microscope under a 10x dry objective to image spheroids, the latter were transferred into fresh media and optical slices (z=10μm) were acquired immediately (to prevent significant diffusion of the fluorophore out of the spheroid). For simplicity, only radial dependence was assumed. An in-house developed erosion algorithm (with ring width equal to 4μm) was applied on the images to evaluate the mean radial intensities and to generate the ratios of the intensities as a function of position. Using the calibration curve of SNARF-4F in media at known pH values at identical imaging conditions, the ratios were then converted to pH_e values in spheroids. Errors correspond

to standard deviations of n=3 independent liposome preparations. Errors correspond to standard deviations of n=3 independent spheroid runs of n=3 spheroids per run.

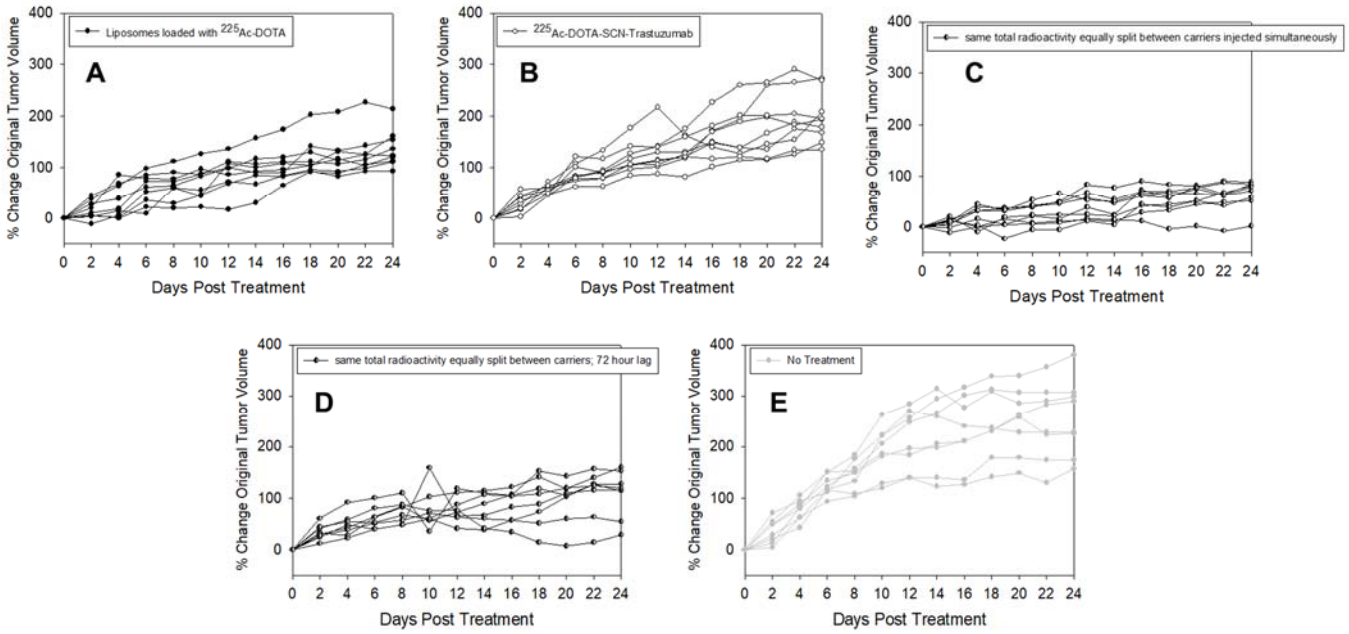

SUPPLEMENTAL FIGURE 7. Volume progression of HER2-positive BT474 orthotopic xenografts on individual NCR nu/nu female mice following a single I.V. administration (at t = 0) of 9.25 kBq per 20g mouse of ^{225}Ac delivered **(A)** by the tumor-responsive liposomes loaded with ^{225}Ac-DOTA alone (black circles), **(B)** by the radiolabeled Trastuzumab alone (^{225}Ac-DOTA-SCN-antibody, 2.96 MBq/mg specific radioactivity in injectate) (white circles), **(C)** by both carriers at equally split (same total) radioactivity injected simultaneously (half-black-half-white circles), and **(D)** by both carriers at equally split (same total) radioactivity with the radiolabeled antibody being administered 72 hours *after* the liposomes (to largely allow for the clearance of the latter from the liver and spleen) (half-black-half-gray circles). Tumors of animals in the non-treated group are indicated by gray circles in plot **(E)**.

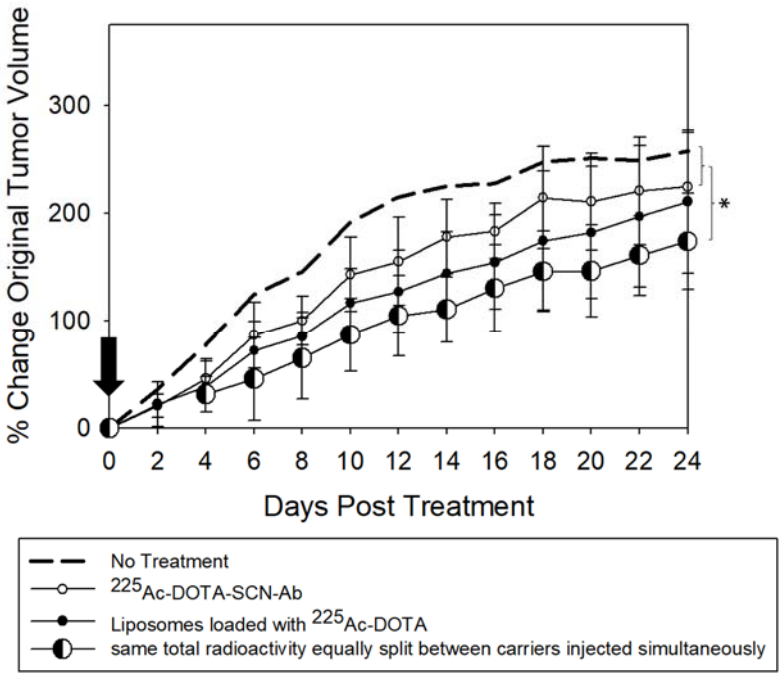

SUPPLEMENTAL FIGURE 8. Volume progression of HER2-positive BT474 orthotopic xenografts on NCR nu/nu female mice following a single I.V. administration (at t=0 indicated by the black arrow) of 4.63 kBq per 20g mouse of ^{225}Ac delivered by the radiolabeled trastuzumab alone (^{225}Ac-DOTA-SCN-antibody, 2.96 MBq/mg specific radioactivity in injectate) (white circles), the tumor-responsive liposomes loaded with ^{225}Ac-DOTA alone (black circles), and by both carriers at equally split (same total) radioactivity injected simultaneously (half-black-half-white circles). Non-treated group is indicated by the dashed line. Data points are the mean values and error bars the standard deviations of n=8–9 animals per group. Significance was calculated with one-way ANOVA (p-value<0.05). * indicates 0.01< p-values <0.05.

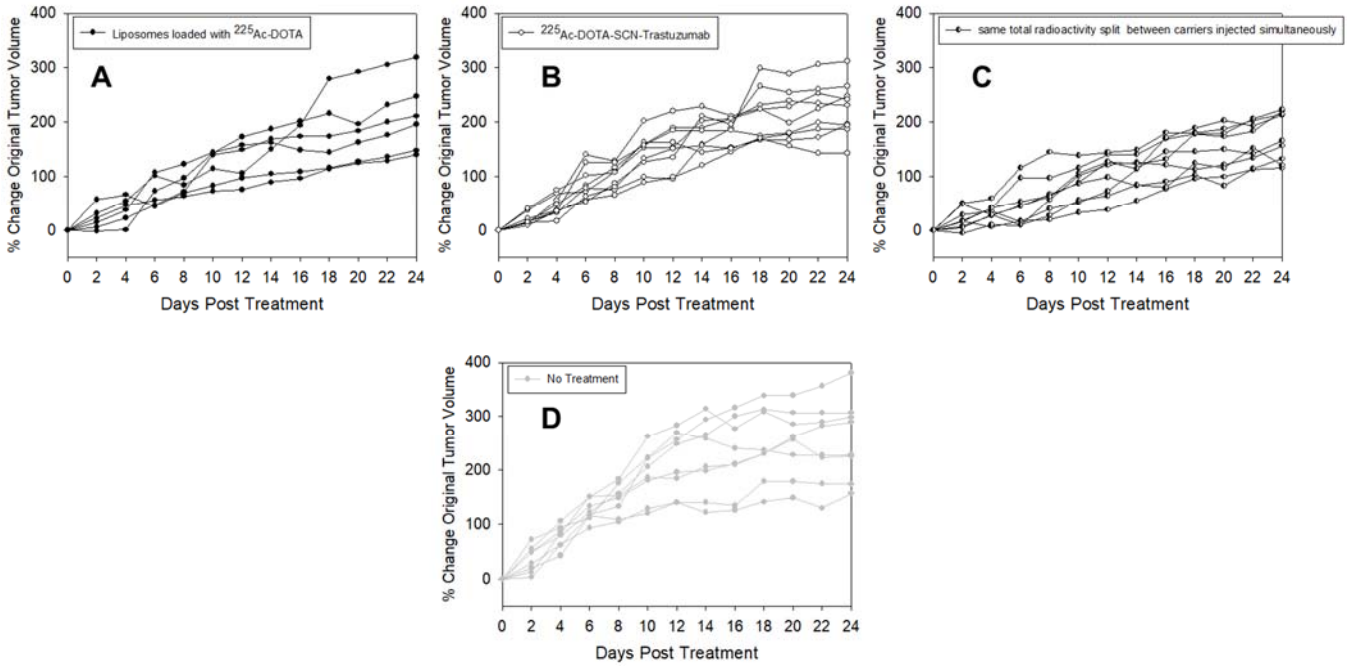

SUPPLEMENTAL FIGURE 9. Volume progression of HER2-positive BT474 orthotopic xenografts on individual NCR nu/nu female mice following a single I.V. administration (at t = 0) of 4.63 kBq per 20g mouse of ^{225}Ac delivered **(A)** by the tumor-responsive liposomes loaded with ^{225}Ac-DOTA alone (black circles), **(B)** by the radiolabeled Trastuzumab alone (^{225}Ac-DOTA-SCN-antibody, 2.96 MBq/mg specific radioactivity in injectate) (white circles), and **(C)** by both carriers at equally split (same total) radioactivity injected simultaneously (half-black-half-white circles). Tumors of animals in the non-treated group are indicated by gray circles in plot **(D)**.

SUPPLEMENTAL FIGURE 10. Treatment study: Normal tissue H&E images from BT474 tumor-bearing NCR nu/nu female mice treated with tumor-responsive liposomes loaded with ^{225}Ac-DOTA and/or ^{225}Ac-DOTA-SCN HER2-targeting Trastuzumab at a total (single I.V.) dose equal to 9.25 kBq per 20g animal.

Histopathology analysis of H&E stained sections of the organs of tumor-bearing mice showed no noteworthy hepatic, cardiac, or renal toxicities across all constructs at the time of sacrifice. Slight inflammation in the diaphragm of the liposome-only treatment group was observed, but otherwise there was no visible lung inflammation. Additionally, increased cell death in and reduced size of the spleen was observed in the liposome-only condition.

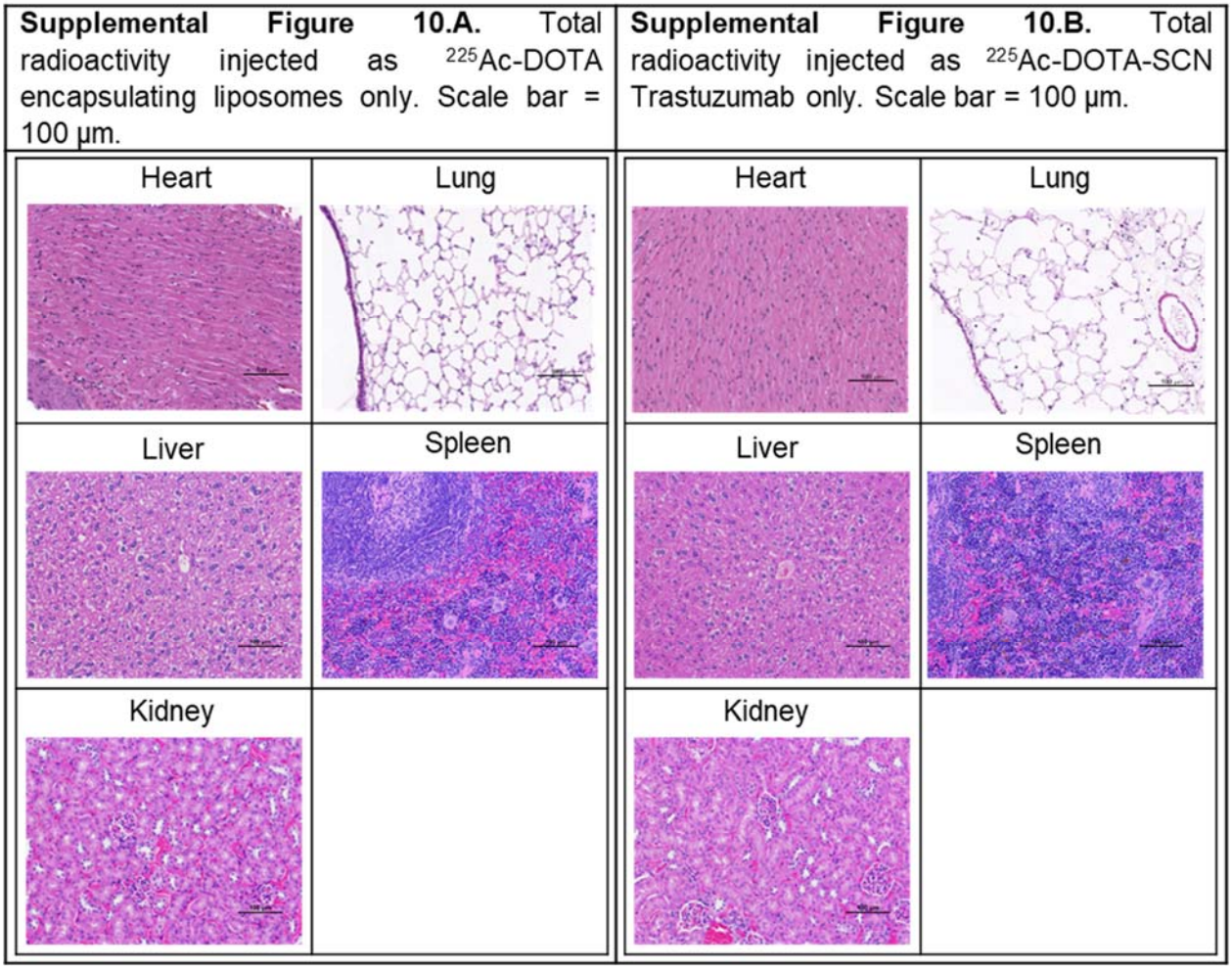

Supplemental Figure 10.A. Total radioactivity injected as ^{225}Ac-DOTA encapsulating liposomes only. Scale bar = 100 µm.

Supplemental Figure 10.B. Total radioactivity injected as ^{225}Ac-DOTA-SCN Trastuzumab only. Scale bar = 100 µm.

Supplemental Figure 10.C. Total radioactivity injected 50% as ^{225}Ac-DOTA encapsulating liposomes and 50% as ^{225}Ac-DOTA-SCN-Trastuzumab. Scale bar = 100 µm.

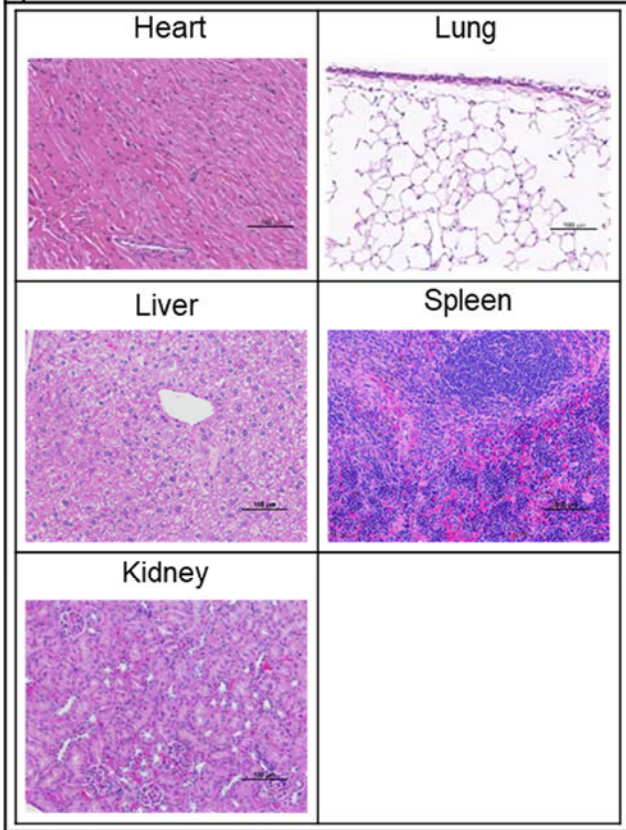

Supplemental Figure 10.D. No treatment. Scale bar = 100 µm.

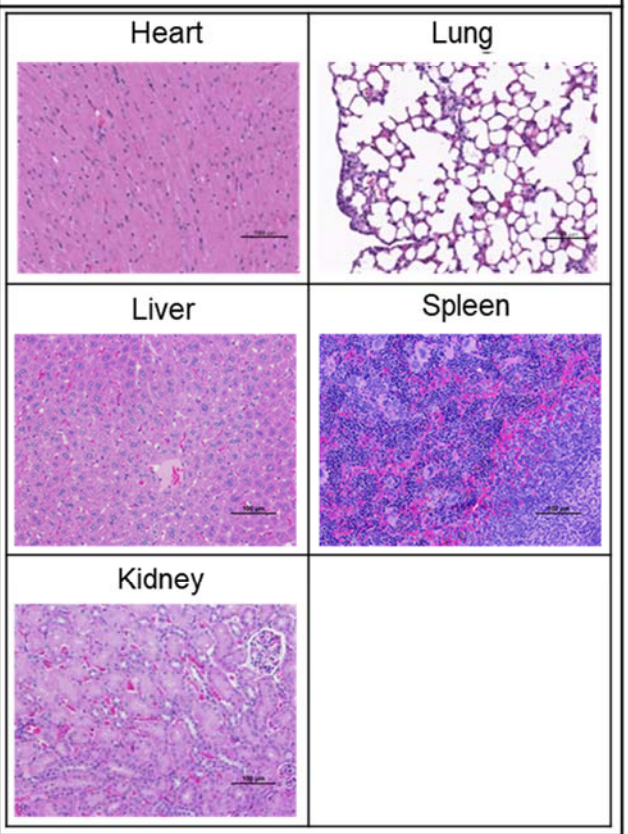

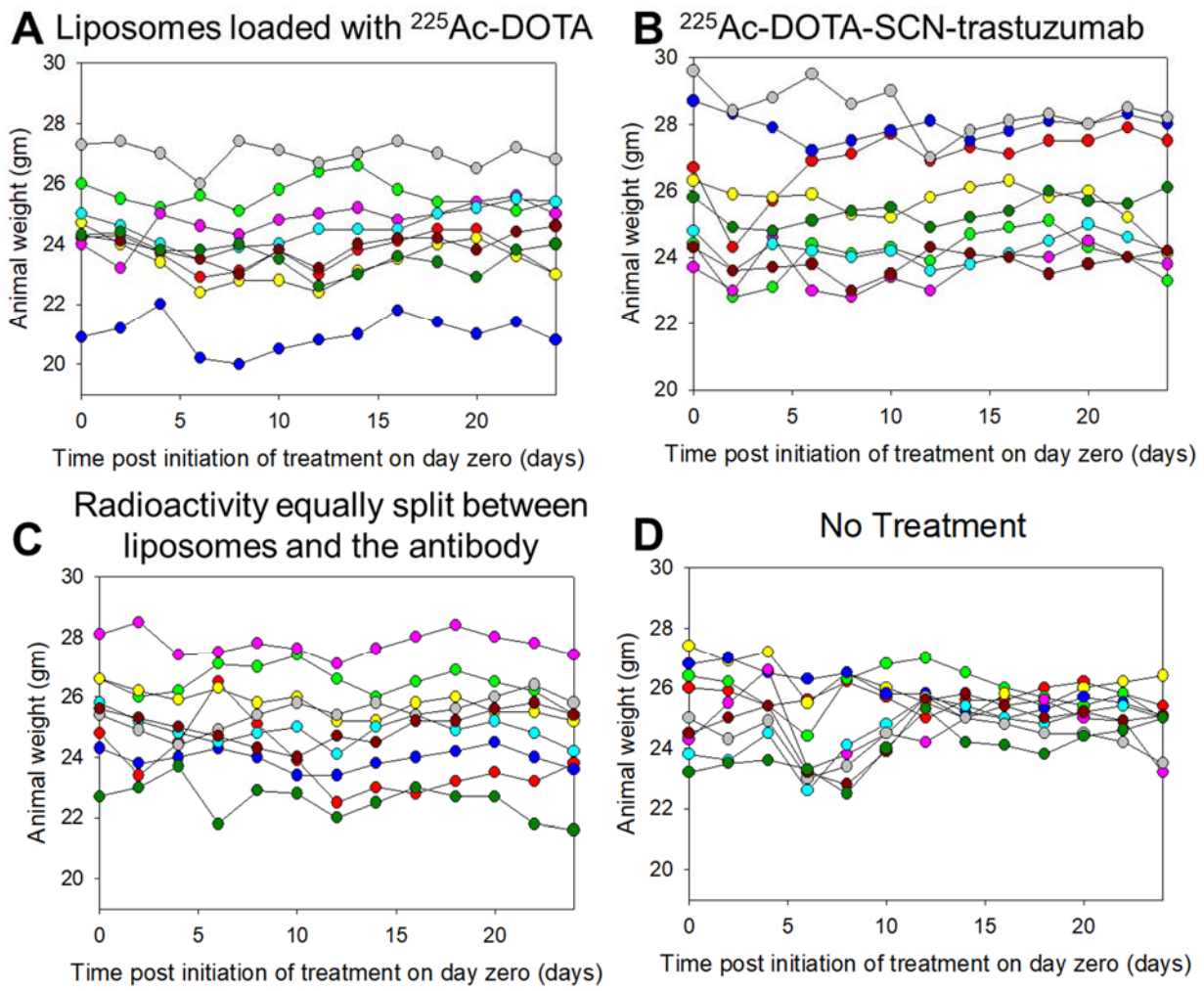

SUPPLEMENTAL FIGURE 11. Treatment study: weight of individual animals during the tumor growth control study. BT474 tumor-bearing NCR nu/nu female mice were injected I.V. with a single total administration equal to 9.25kBq per 20g animal on day 0 in the following forms: **(A)** ^{225}Ac-DOTA encapsulating tumor-responsive liposomes, **(B)** ^{225}Ac-DOTA-SCN Trastuzumab, and **(C)** no treatment, and **(D)** same total radioactivity equally split between ^{225}Ac-DOTA encapsulating liposomes and ^{225}Ac-DOTA-SCN Trastuzumab. Animal weight was monitored every other day, and did not decrease beyond 10% of original weight during the treatment study.

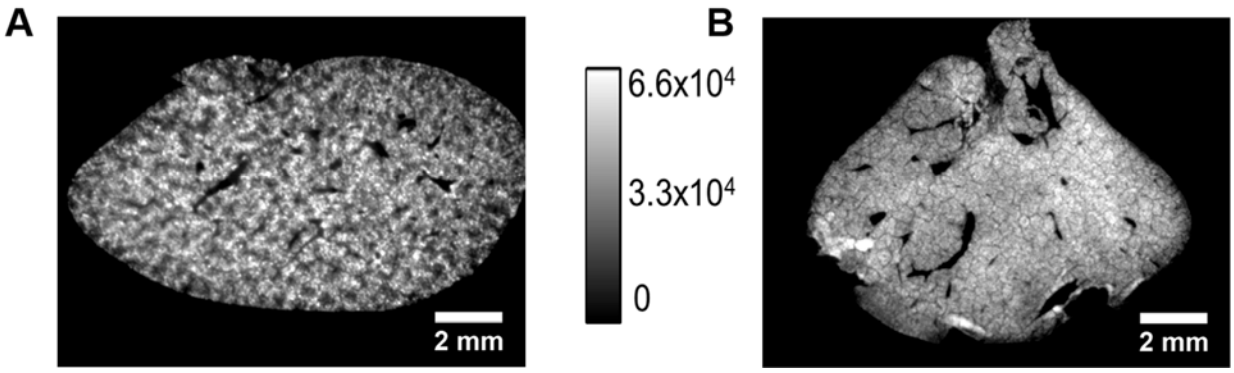

SUPPLEMENTAL FIGURE 12. Decay-corrected α-Camera images of liver sections from NCR nu/nu female mice collected 24 hours upon I.V. administration showing the spatial distributions of ^{225}Ac delivered by **(A)** ^{225}Ac-DOTA encapsulating tumor-responsive liposomes, and **(B)** ^{225}Ac-DOTA-SCN-trastuzumab. Scale bar = 2mm. The spatial micro-distributions of ^{225}Ac were less uniform (and more grainy) when delivered by liposomes, compared to when delivered by the antibody.

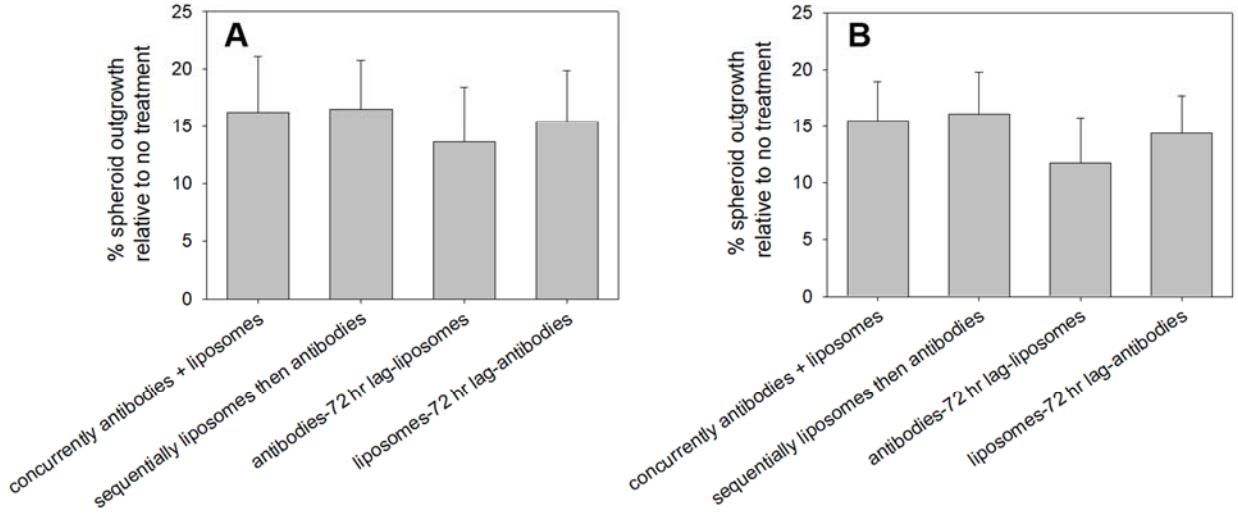

SUPPLEMENTAL FIGURE 13. Variation in the delivery schedule of same total radioactivity and same radioactivity split ratio between the ^{225}Ac-DOTA encapsulating tumor-responsive liposomes and ^{225}Ac-DOTA-SCN-Trastuzumab did not result in statistically different extents of spheroid outgrowth control in 400 μm-in diameter spheroids following treatment with either **(A)** 13.75kBq/mL or **(B)** 18.5kBq/mL. (n = 4-5 spheroids per condition, 2 independent preparations.)